



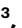








Platelet glycoprotein V spatio-temporally controls fibrin formation

Received: 23 May 2022

Accepted: 15 February 2023

Published online: 23 March 2023

 Check for updates

Sarah Beck ^{1,2}, Patricia Öftering ^{1,2}, Renhao Li ³, Katherina Hemmen ¹,
Magdolna Nagy⁴, Yingchun Wang³, Alessandro Zarpellon⁵,
Michael K. Schuhmann⁶, Guido Stoll⁶, Zaverio M. Ruggeri ⁵,
Katrin G. Heinze ¹, Johan W. M. Heemskerk⁴, Wolfram Ruf ^{7,8,9},
David Stegner ^{1,2,9}  & Bernhard Nieswandt ^{1,2,9} 

The activation of platelets and coagulation at vascular injury sites is crucial for hemostasis but can promote thrombosis and inflammation in vascular pathologies. Here, we delineate an unexpected spatio-temporal control mechanism of thrombin activity that is platelet orchestrated and locally limits excessive fibrin formation after initial hemostatic platelet deposition. During platelet activation, the abundant platelet glycoprotein (GP)V is cleaved by thrombin. We demonstrate, with genetic and pharmacological approaches, that thrombin-mediated shedding of GPV does not primarily regulate platelet activation in thrombus formation but rather has a distinct function after platelet deposition and specifically limits thrombin-dependent generation of fibrin, a crucial mediator of vascular thrombo-inflammation. Genetic or pharmacologic defects in hemostatic platelet function are unexpectedly attenuated by specific blockade of GPV shedding, indicating that the spatio-temporal control of thrombin-dependent fibrin generation also represents a potential therapeutic target to improve hemostasis.

Hemostasis is the physiological mechanism that limits bleeding after blood vessel injury through intertwined activation of circulating platelets and the plasmatic coagulation cascade¹. The adhesion of platelets to extracellular matrix proteins and von Willebrand factor (VWF) initiates the hemostatic response that is supported by exposure of subendothelial tissue factor (TF), which triggers coagulation and local thrombin generation². This results in a fibrin network encasing platelets in a stable thrombus³. Thrombin generation requires feed-forward reactions that involve platelet activation by thrombin-mediated cleavage and activation of G protein-coupled protease-activated receptors

(PARs)⁴ and amplification of coagulation reactions on the surface of activated platelets⁵. Generated thrombin forms fibrin and thereby stabilizes thrombi through platelet receptor GPIIb/GPIIIa engagement and activates factor XIII (FXIII) to cross-link fibrin fibers⁶. These processes are regulated with high fidelity⁷ to ensure efficient hemostasis while preventing thrombosis and thrombo-inflammatory diseases^{8,9}. In addition, thrombin activity in the circulation is limited by specific plasmatic coagulation inhibitors and by thrombomodulin on endothelial cells, which captures thrombin to initiate the coagulation-regulatory and vascular-protective protein C pathway¹⁰.

¹Rudolf Virchow Center for Integrative and Translational Bioimaging, Julius-Maximilians-Universität Würzburg, Würzburg, Germany. ²Institute of Experimental Biomedicine, University Hospital Würzburg, Würzburg, Germany. ³Aflac Cancer and Blood Disorders Center, Children's Healthcare of Atlanta, Department of Pediatrics, Emory University School of Medicine, Atlanta, GA, USA. ⁴Department of Biochemistry, CARIM, Maastricht University, Maastricht, the Netherlands. ⁵Department of Molecular Medicine, Scripps Research, La Jolla, CA, USA. ⁶Department of Neurology, University Hospital Würzburg, Würzburg, Germany. ⁷Center for Thrombosis and Hemostasis, Johannes Gutenberg University Medical Center Mainz, Mainz, Germany. ⁸Department of Immunology and Microbiology, Scripps Research, La Jolla, CA, USA. ⁹These authors contributed equally: Wolfram Ruf, David Stegner, Bernhard Nieswandt. ✉ e-mail: stegner@virchow.uni-wuerzburg.de; bernhard.nieswandt@virchow.uni-wuerzburg.de

The GPIb–GPIX complex mediates platelet binding to VWF and is crucial for hemostasis. Mutations in *GP1BA*, *GP1BB* or *GP9* cause Bernard–Soulier syndrome, a rare bleeding disorder characterized by giant platelets^{11,12}. GPV is associated with the GPIb–GPIX complex but is not required for GPIb expression or functional interactions¹³. GPV is an abundant 88-kDa platelet- and megakaryocyte-specific leucine-rich repeat transmembrane protein¹⁴ that interacts with collagen¹⁵ and has minor importance for platelet function^{16,17}. GPV is proteolytically cleaved by thrombin during thrombus formation^{18,19}, but the physiological roles of the shed 69-kDa extracellular fragment in hemostasis and thrombosis has remained elusive.

Results

Thrombus formation is accelerated in *Gp5*-mutant mice

We studied the role of GPV in thrombus formation by comparing wild-type (WT) and *Gp5*^{-/-} mice in FeCl₃-induced thrombosis of mesenteric arterioles in vivo. In line with previous observations²⁰, *Gp5*^{-/-} mice displayed faster onset of thrombus formation and shortened occlusion times without increased embolization, indicating a prothrombotic phenotype in the absence of GPV (Fig. 1a,b). Platelet hyper-reactivity to thrombin is the presumed but unproven mechanism for enhanced thrombosis in *Gp5*^{-/-} mice and is thought to be related to thrombin-mediated cleavage of GPV. To directly study the relevance of thrombin-mediated GPV cleavage, we generated a mouse carrying a point mutation in the thrombin cleavage site of GPV (*Gp5*^{dThr}; Extended Data Fig. 1a). Platelets of these mice showed unaltered surface expression levels of GPV compared to those of WT mice, and GPV was completely resistant to cleavage by thrombin (Extended Data Fig. 1b,c and Extended Data Table 1). By contrast, cleavage of the mutant GPV by endogenous a disintegrin and metalloproteinase (ADAM)17 (ref. 21) was not affected (Extended Data Fig. 1b–e), demonstrating the thrombin specificity of the *Gp5*^{dThr} mutation. Unexpectedly, *Gp5*^{dThr} mice displayed accelerated thrombus formation in the FeCl₃ arteriolar injury model and, in this respect, resembled *Gp5*^{-/-} mice (Fig. 1c,d).

In a series of experiments, we addressed the possibility that excessive platelet activation also caused the prothrombotic phenotype of *Gp5*^{dThr} mice. Loss of surface GPV led to hyper-reactivity of *Gp5*^{-/-} platelets specifically at lower thrombin concentrations but not with other agonists (Fig. 1e,g,h and Extended Data Fig. 1f–h), as previously shown^{15,20,22–24}. In sharp contrast to *Gp5*^{-/-} platelets, measurements of P-selectin exposure (Fig. 1f) and α_{IIb}β₃ integrin activation and platelet aggregation (Fig. 1g,h and Extended Data Fig. 1i) showed that *Gp5*^{dThr} platelets were not hyper-reactive at the threshold thrombin concentration. Of note, both *Gp5*^{-/-} and *Gp5*^{dThr} platelet-rich plasma (PRP) showed unaltered clot retraction (Extended Data Fig. 1j).

We next tested the hypothesis that membrane-bound GPV might act as a regulator of thrombin-mediated PAR activation²⁵, supported by the high-affinity binding of thrombin for GPIbα^{26,27}. Blockade of the GPIbα–thrombin interaction on mouse platelets with Fab fragments of the anti-GPIbα antibody pOp/B^{28,29} (Extended Data Fig. 2a) indeed diminished platelet activation, particularly at low thrombin concentrations (Extended Data Fig. 2c). Although human and mouse platelets are activated by thrombin through different PARs, these antibody inhibition data indicated that mouse platelets are similar to human platelets²⁵ in requiring GPIbα for thrombin-induced activation at threshold agonist concentrations. Remarkably, the anti-GPIbα antibody completely abolished the enhanced activation of *Gp5*^{-/-} platelets relative to WT platelets (Extended Data Fig. 2c), implying that loss of GPV sensitized to GPIbα-dependent thrombin signaling. By contrast, activation of *Gp5*^{dThr} platelets at threshold concentrations of thrombin was indistinguishable from that of WT platelets with or without anti-GPIbα pOp/B (Extended Data Fig. 2b,c). Thus, surface GPV regulates platelet responsiveness to thrombin primarily by interference with GPIbα-dependent PAR signaling in mouse platelets (Extended Data Fig. 2d,e).

The delineated pathway of enhanced in vitro thrombin signaling in *Gp5*^{-/-} platelets could not explain the similar prothrombotic phenotype of *Gp5*^{-/-} and *Gp5*^{dThr} mice in vivo, suggesting that shed GPV regulates thrombus formation by a mechanism unrelated to the regulation of platelet activation following vascular injury. We therefore next asked whether platelet procoagulant function might be regulated by GPV. Measurements of TF-initiated thrombin generation in PRP did not, however, uncover differences between *Gp5*^{-/-}, *Gp5*^{dThr} and WT platelets (Extended Data Fig. 2f–k), in line with previous results from GPV-deficient platelets¹², excluding alterations in platelet membrane procoagulant activity.

We next evaluated whether the known collagen interaction of GPV might contribute to thrombus growth modulation by GPV. Platelet activation is triggered through two major signaling pathways. Specifically, soluble agonists, including thrombin and secondary mediators ADP and thromboxane A₂, act through G protein-coupled receptors, whereas immobilized and/or multimeric ligands signal through immunoreceptor tyrosine-based activation motif (ITAM)-coupled receptors, C-type lectin-like receptor 2 (CLEC-2) and GPVI. Platelet GPVI is the major activating collagen receptor, and GPVI deficiency and antagonism protect from arterial thrombosis with more moderate effects on hemostasis³⁰. We analyzed thrombus formation in the absence or presence of platelet GPVI to uncover potential collagen-binding functions of GPV. GPVI was immunodepleted from platelets by injection of the anti-GPVI antibody JAQ1 (ref. 31) 5 d before inducing FeCl₃ mesenteric arteriole injury (Extended Data Fig. 3a,b). As reported previously³¹, GPVI depletion markedly attenuated occlusive thrombus formation in WT mice in vivo. Surprisingly, loss of GPVI was without effect in the absence of GPV, and the shortened occlusion times of *Gp5*^{-/-} mice persisted even after GPVI depletion in two distinct vascular beds (Extended Data Fig. 3c–e).

In addition, GPV deficiency prevented the prolongation of the bleeding time associated with GPVI depletion in WT animals (Extended Data Fig. 3f). These data essentially excluded the possibility that GPV regulated GPVI–collagen interaction or contributed to collagen-dependent platelet activation under these experimental conditions. Rather, GPV deficiency over-ruled the hemostatic and thrombotic defects caused by the absence of GPVI and restored thrombus formation in vivo. It has previously been shown that functional defects related to GPVI–ITAM-mediated platelet activation can be attenuated by increased local thrombin generation in different vascular beds³², and mouse GPVI does not interact with mouse fibrinogen³³. Thus, the demonstrated reversal of GPVI inhibition in *Gp5*^{-/-} mice suggested that soluble GPV (sGPV) regulated thrombin activity during thrombus formation.

sGPV binds to thrombin and localizes to fibrin

We therefore evaluated the role of GPV in thrombin-mediated fibrin formation on collagen–TF spots in recalcified whole blood under flow in vitro³⁴. Time to fibrin formation was shortened and the overall amount of fibrin generated was increased in *Gp5*^{-/-} mice (Fig. 2a–c) and, importantly, also in *Gp5*^{dThr} mice (Fig. 2d–f) compared to WT controls. Quantitative imaging of formed thrombi and generated fibrin³⁵ showed increased thrombus height, based on multilayer and contraction scores, as well as fibrin formation, based on fibrin surface coverage and fibrin score, in the blood of both mutant mouse lines (Fig. 2g). Of note, this ex vivo experimental setup produced results entirely in line with the in vivo findings that *Gp5*^{-/-} and *Gp5*^{dThr} mice concordantly displayed accelerated thrombus formation.

These data indicate that cleavage of GPV is a critical step in an autoregulatory limitation of fibrin generation. Thrombin binds to de novo generated fibrin via the regulatory thrombin exosites I and II and thereby becomes protected from coagulation inhibitors in the blood³⁶. We hypothesized that sGPV directly or indirectly affected thrombin–fibrin interactions. We first evaluated the direct interaction of sGPV

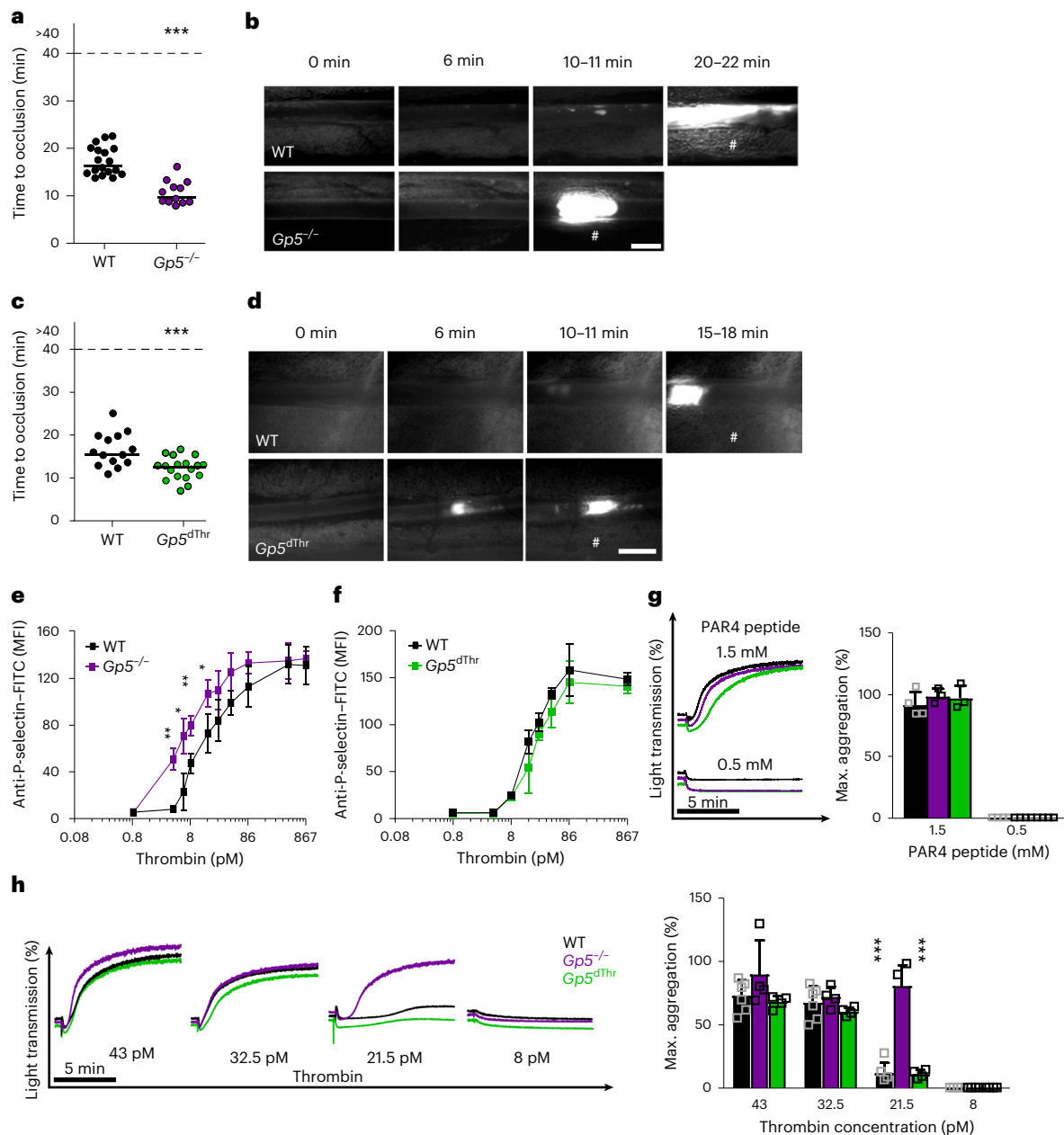


Fig. 1 | Platelet thrombin hyper-responsiveness and accelerated thrombus formation in *Gp5* mutant mice. Quantification (a) and representative images (b) of thrombus formation upon FeCl_3 -induced injury of mesenteric arterioles in *Gp5*^{-/-} or WT mice. Thrombus formation in no more than two arterioles of each mouse was analyzed; data points represent measurements of one arteriole. Horizontal line represents mean. WT, $n = 18$ arterioles of 11 mice; *Gp5*^{-/-}, $n = 12$ arterioles of seven mice; two-tailed unpaired t -test, $P < 0.0001$. Scale bar, 50 μm . Quantification of thrombus formation (c) and representative images (d) upon FeCl_3 -induced injury of mesenteric arterioles in *Gp5*^{dThr} or WT mice. Horizontal line represents mean. Horizontal dashed line in a and c indicates the end of the experiment. At most, two arterioles of each mouse were analyzed. Each dot represents one arteriole. The symbol # indicates occlusive thrombus formation. WT, $n = 14$ arterioles of ten mice; *Gp5*^{dThr}, $n = 18$ arterioles of nine mice; two-tailed unpaired t -test, $P = 0.0010$. Scale bar, 50 μm . e, Increased P-selectin exposure of GPV-deficient platelets at threshold thrombin concentrations. Mean \pm s.d., $n = 4$

mice per group, five independent experiments, two-tailed unpaired t -test with Welch's correction. P values: 4.3 pM thrombin, $P = 0.0025$; 6.45 pM thrombin, $P = 0.0286$; 8.6 pM thrombin, $P = 0.0020$; 17.2 pM thrombin, $P = 0.0179$. MFI, mean fluorescence intensity. f, Flow cytometry reveals unaltered reactivity of *Gp5*^{dThr} platelets upon thrombin stimulation compared to WT controls. Mean \pm s.d., $n = 4$ mice per group, five independent experiments. g, h, Washed platelets were stimulated with the indicated agonists, and light transmission of washed platelets upon stimulation with the PAR4 peptide (g) or thrombin (h) at the indicated concentrations was recorded on an APACT four-channel aggregometer over 10 min. Representative curves for $n = 4$ (g), $n = 4$ (h) (*Gp5*^{-/-}; *Gp5*^{dThr}) and $n = 4$ –6 for WT of three independent experiments. Maximum (max.) aggregation is expressed as mean \pm s.d. WT versus *Gp5*^{-/-} and *Gp5*^{-/-} versus *Gp5*^{dThr}, $P < 0.0001$. One-way ANOVA followed by Tukey's multiple-comparison test. Strain-matched controls were used. * $P < 0.05$, ** $P < 0.01$, *** $P < 0.001$.

and thrombin. We stimulated platelets with biotinylated thrombin and showed that sGPV coprecipitated in the thrombin pull-down using streptavidin-coated beads (Fig. 2h), consistent with direct interaction of thrombin with sGPV.

Because GPV release was required to attenuate fibrin formation of recalcified whole blood perfused over collagen-TF spots (Fig. 2a–f), we next quantified the colocalization of GPV with fibrin in this setting. Using confocal microscopy with super-resolution mode, we excluded

in the image analysis platelet-rich areas based on GPIX staining and subsequently quantified the colocalization of GPV with fibrin (Fig. 2i,j and Supplementary Fig. 1). Quantification of GPV intensities showed that GPV accumulated with fibrin in platelet-free areas of thrombi (Fig. 2j).

Based on these data, we reasoned that, upon initiation of a hemostatic platelet response, thrombin-mediated cleavage of GPV formed sGPV–thrombin complexes, which limited thrombin diffusion and activity in the forming fibrin clot. To test this concept, we recombinantly expressed the ectodomain of human GPV using a construct that included the thrombin cleavage site (rhGPV) (Fig. 3a). Aggregation of rhGPV at high concentrations prevented us from performing experiments with full dose–response curves. However, thrombin-mediated platelet activation was only marginally inhibited by 290 nM (20 $\mu\text{g ml}^{-1}$) rhGPV at threshold thrombin concentrations (Extended Data Fig. 4a,b), in line with the conclusion that platelet activation by thrombin is primarily regulated by membrane-bound GPV. In sharp contrast, rhGPV at the same concentration impaired fibrin formation in a static polymerization assay (Fig. 3b and Extended Data Fig. 4c,d) triggered specifically by thrombin, whereas fibrin polymerization induced by another protease, batroxobin, was unaltered in the presence of rhGPV (Fig. 3b and Extended Data Fig. 4c,d). Importantly, sGPV localized to fibrin polymers independent of the clot-inducing enzyme, indicating direct interactions of GPV with fibrin independent of thrombin–GPV complex formation.

These data also indicate that sGPV in the developing clot directly inhibits thrombin's activity to form fibrin. We therefore studied the interaction of rhGPV with thrombin in the absence of fibrinogen. Incubation of equimolar concentrations of thrombin with rhGPV containing the thrombin cleavage site resulted in time-dependent rhGPV proteolysis, demonstrating that GPV is a thrombin substrate independent of anchoring to the platelet surface (Extended Data Fig. 4e–g). However, formation of sGPV stopped after 5–10 min, when approximately 50% of the substrate was consumed. Measurements of thrombin activity toward a chromogenic substrate were unchanged during the reaction time, excluding instability of the enzyme (Extended Data Fig. 4g). Of note, at the end of the incubation time, sGPV still inhibited thrombin's activity to form fibrin (Extended Data Fig. 4h–j). To distinguish between substrate depletion and product inhibition, we performed the same reaction with a tenfold higher substrate concentration. This reaction yielded essentially the same amount of product, implying that the generated sGPV caused product inhibition and interacted with thrombin independent of fibrin binding. Attempts to chemically cross-link sGPV and thrombin under these conditions were unsuccessful, suggesting that the required amino groups were not in close enough proximity.

Fig. 2 | GPV alters fibrin formation and localizes to fibrin fibers outside the thrombus after thrombin cleavage.

a, Time-dependent fibrin generation of $Gp5^{-/-}$ and WT mice was quantified. Mean \pm s.e.m.; WT, $n = 9$; $Gp5^{-/-}$, $n = 8$; three independent experiments. Two-tailed unpaired *t*-test with Welch's correction. *P* values: 4.5 min, $P = 0.0072$; 5.5 min, $P = 0.0296$; 6 min, $P = 0.0006$. **b**, Representative images of thrombus formation (anti-GPIX–Alexa Fluor (AF)647 antibody, red) and fibrin formation (fibrin(ogen)–AF488, green) on collagen–TF spots after 6 min. Scale bar, 20 μm . **c**, Quantification of time to fibrin formation. Each dot represents one animal. Mean \pm s.d., $n = 4$, two-tailed Mann–Whitney test. $P = 0.0286$. **d–f**, Fibrin formation on collagen–TF microspots of $Gp5^{\text{dThr}}$ and WT mice. Quantification of fibrin formation (**d**), time to fibrin formation (**f**) and representative images (**e**). Scale bar, 20 μm . For staining, see **b**. **d**, Mean \pm s.e.m.; WT, $n = 6$; $Gp5^{\text{dThr}}$, $n = 8$; two-tailed unpaired *t*-test with Welch's correction. *P* values: 6 min, $P = 0.0287$. **f**, Mean \pm s.d.; WT, $n = 5$; $Gp5^{\text{dThr}}$, $n = 4$; two-tailed Mann–Whitney test. $P = 0.0317$. SAC, surface area coverage. Horizontal dashed line in **c** and **f** indicates the end of the experiment; every dot above it did not show any occlusion/fibrin formation within the observation period. **g**, Subtraction heatmap of parameters of thrombus (increased multilayer and contraction score) and fibrin formation in mutant mice compared to WT controls. Colors

rhGPV reduces fibrin formation and protects from thrombosis

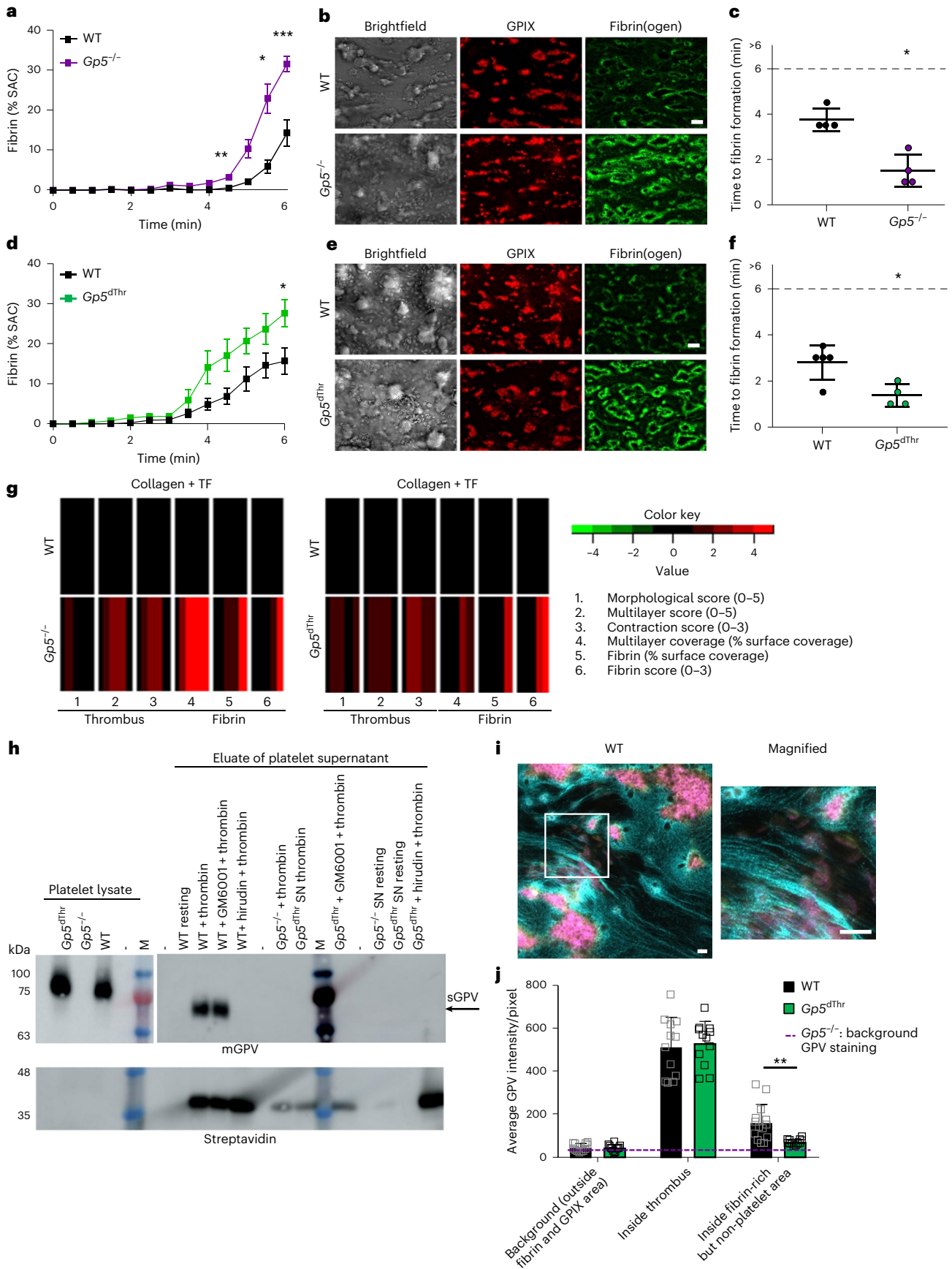
In addition, rhGPV impaired fibrin formation in human (Extended Data Fig. 5a–c) and mouse blood (Extended Data Fig. 5d–g) in the collagen–TF-induced thrombus-formation assay under flow, supporting a role for sGPV in limiting thrombin activity toward fibrin. Analysis of the formed fibrin fibrils by confocal microscopy revealed a fine, dense and branched network consisting of thin, clearly distinguishable fibers in control samples, whereas fibers were generally thicker but less frequent and structurally less defined in the presence of rhGPV (Extended Data Fig. 5f), confirming that rhGPV impedes fibrin formation. Of note, a His-tagged fusion protein did not reduce fibrin formation, demonstrating specificity of the recombinant GPV.

We next measured thrombin activity in the outflow of the flow chamber and found that less thrombin activity was recovered in rhGPV-treated samples compared to controls (Extended Data Fig. 5h). Conversely, we found more thrombin in the outflow of the chambers perfused with $Gp5^{-/-}$ and $Gp5^{\text{dThr}}$ versus WT blood (Extended Data Fig. 8a), further supporting the conclusion that sGPV controls thrombin activity specifically in fibrin clots. We next imaged thrombin activity in flow chambers cleared of blood by perfusion with Tyrode's buffer and the thrombin substrate Z-GGR-AMC. We found reduced thrombin activity in clots formed in the presence of rhGPV (Extended Data Fig. 5i,j). In sum, these data support a role for GPV in retaining thrombin in fibrin clots and limiting thrombin's activity in fibrin formation.

We next tested whether rhGPV could modulate thrombus formation *in vivo*. Indeed, a single intravenous dose of 20 μg rhGPV before thrombosis induction reduced arterial thrombus formation in two different experimental models. In a model of mechanical injury to the abdominal aorta in which blood flow and occlusive thrombus formation were monitored by an ultrasonic flow probe (Fig. 3c and Extended Data Fig. 5k), 14 of 15 mice did not form stable thrombi after rhGPV administration within the observation period of 30 min, whereas 18 of 18 arteries occluded in the control group. In FeCl_3 -induced mesenteric arteriole injury, time to occlusion was markedly prolonged in mice treated with rhGPV (Fig. 3d,e).

In addition, rhGPV treatment provided protection from thrombo-inflammatory neurological damage and improved neurological outcome in the transient middle cerebral artery (MCA) occlusion (tMCAO) model of ischemic stroke (Fig. 3f–h) in which the concerted action of platelets, the coagulation system and immune cells is known to drive post-ischemic cerebral infarct growth³⁷. Of note, infarct volumes of $Gp5^{-/-}$ and $Gp5^{\text{dThr}}$ mice after tMCAO were comparable to those of WT mice (Fig. 3f–g), suggesting that thrombin activity in WT mice is already above threshold values needed to fully promote infarct progression under these experimental conditions. Importantly, no large intracranial

represent unchanged (black), decreased (green) or increased (red) parameters. **h**, Pull-down of sGPV from WT platelets using streptavidin beads after stimulation with biotinylated thrombin in the presence or absence of GM6001 (matrix metalloproteinase inhibitor). Pull-down of sGPV was not observed from $Gp5^{\text{dThr}}$ platelets or in the presence of hirudin, which prevents GPV cleavage by thrombin. Eluates were analyzed by western blotting using GPV-specific antibodies and streptavidin–horseradish peroxidase (HRP). Representative results of five independent experiments are shown. M, marker; mGPV, murine GPV; SN, supernatant; arrow indicates pull-down of sGPV. **i,j**, Recalcified blood was perfused over collagen–TF microspots. Samples were stained for platelets (anti-GPIX antibody, yellow), fibrin(ogen) (cyan) and GPV (magenta) and analyzed with a Zeiss Airyscan microscope. **i**, Representative WT image and magnified view. Scale bar, 4 μm . **j**, Quantification of GPV intensities inside fibrin-rich but non-platelet area. Background GPV intensity in $Gp5^{-/-}$ images is displayed as a dashed line. Two-way ANOVA followed by Tukey's multiple-comparison test, $n = 14$ (WT), $n = 12$ ($Gp5^{\text{dThr}}$), $n = 4$ ($Gp5^{-/-}$) regions of interest representing $n = 4$ mice. Mean \pm s.d., $P = 0.0086$. For detailed analysis, see Supplementary Fig. 1. * $P < 0.05$, ** $P < 0.01$, *** $P < 0.001$.



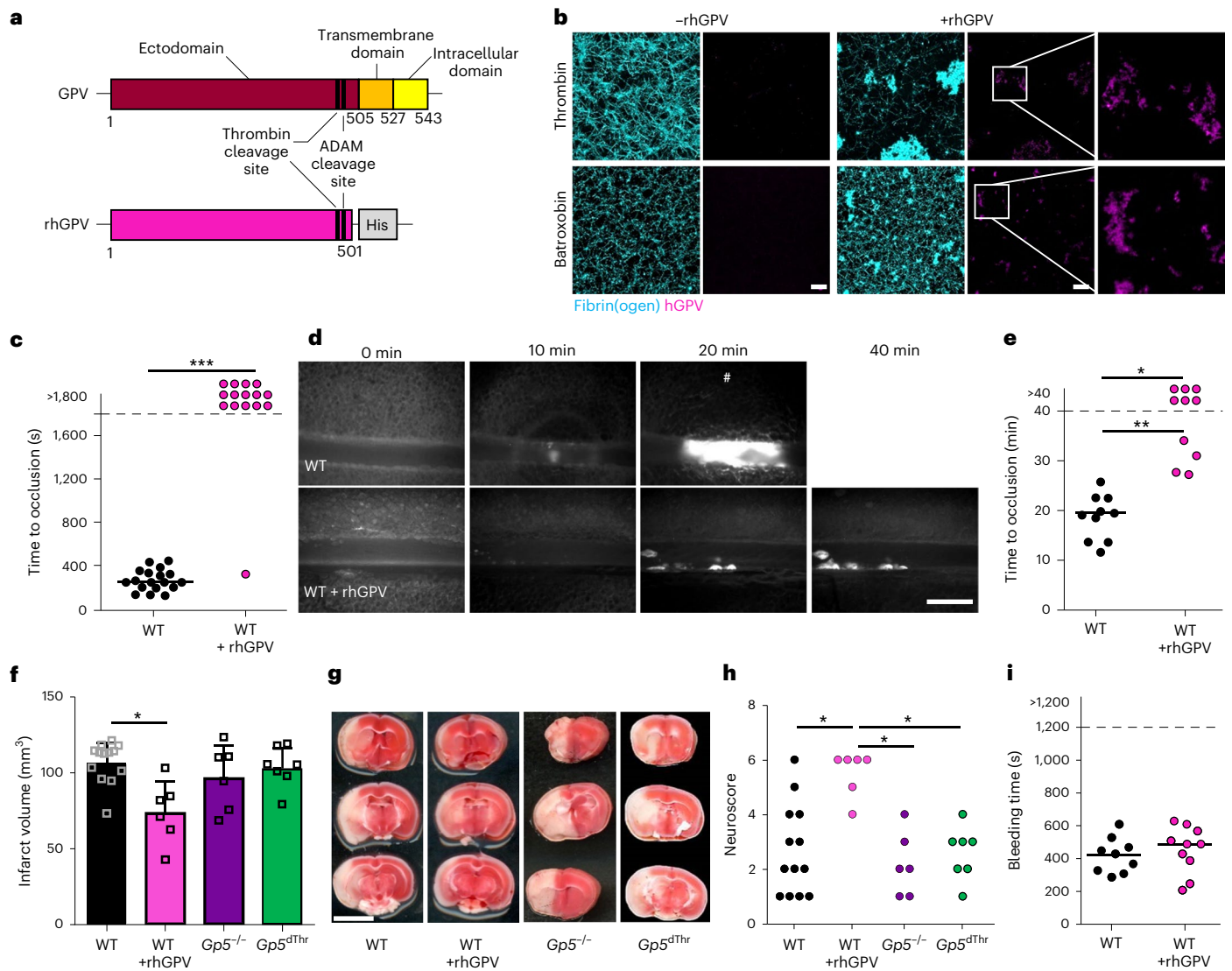


Fig. 3 | rhGPV reduces fibrin formation and thereby protects from occlusive thrombosis and ischemic stroke. **a**, Simplified scheme of the full-length and recombinant ectodomain of human GPV. rhGPV contains the thrombin and ADAM cleavage sites and a C-terminal His-tag. **b**, Maximum projection of static fibrin polymerization induced by thrombin (top) or batroxobin (bottom) in the absence or presence of rhGPV (see Extended Data Fig. 4c,d for quantification). Fluorophore-labeled fibrin(ogen), cyan; staining for hGPV, magenta. Scale bar, 20 μ m. **c**, Quantification of thrombus formation after mechanical injury of the abdominal aorta. WT, $n = 18$; WT + rhGPV, $n = 15$; two-tailed Fisher's exact test, $P < 0.0001$. Representative images (# indicates occlusive thrombus formation; scale bar, 50 μ m) (**d**) and quantification (**e**) of thrombus formation upon FeCl_3 -induced injury of mesenteric arterioles of rhGPV-treated and WT mice. WT, $n = 10$ arterioles of five mice; WT + rhGPV, $n = 10$ arterioles of six mice; two-tailed Fisher's exact test for open versus occluded vessels: WT versus rhGPV, $P = 0.0108$; two-tailed Mann-Whitney test for comparison of occluded vessels, $P = 0.002$.

f, Quantification of infarct volumes in the tMCAO model of ischemic stroke. Mean \pm s.d.; WT, $n = 13$; WT + rhGPV, $n = 6$; $Gp5^{-/-}$, $n = 6$; $Gp5^{\text{dThr}}$, $n = 7$; two-tailed Kruskal-Wallis test with Dunn's post test, $P = 0.0298$. Of note, rhGPV treatment neither triggered large intracranial hemorrhages nor elevated mortality (WT, two of 15; WT + rhGPV, one of seven; $Gp5^{-/-}$, zero of six; $Gp5^{\text{dThr}}$, one of eight). **g**, Three consecutive 2,3,5-triphenyltetrazolium chloride (TTC)-stained brain sections of one representative mouse. White, infarct; red, viable tissue. Scale bar, 0.5 cm. **h**, Neuroscore displaying behavioral outcome after tMCAO. WT versus WT + rhGPV, $P = 0.0135$; WT + rhGPV versus $Gp5^{-/-}$, $P = 0.0116$; WT + rhGPV versus $Gp5^{\text{dThr}}$, $P = 0.0440$; one-way ANOVA followed by Dunn's test for multiple comparisons. **i**, Unaltered tail-bleeding time after rhGPV treatment. WT, $n = 9$; WT + rhGPV, $n = 10$. Horizontal line in **c**, **h** and **i** represents mean. Horizontal dashed line in **c**, **e** and **i** indicates the end of the experiment; every dot above it did not show any occlusion/fibrin formation within the observation period. For rhGPV, 20 μ g per mouse was injected before surgery. * $P < 0.05$, ** $P < 0.01$, *** $P < 0.001$.

hemorrhages were observed in $Gp5^{-/-}$ or $Gp5^{\text{dThr}}$ and rhGPV-treated WT mice (Fig. 3g). Of note, MCA vessel diameters were similar in $Gp5^{-/-}$ and WT mice (Extended Data Fig. 6). In addition, hemostatic function evaluated by the tail-bleeding time assay was also comparable between mice injected with rhGPV and vehicle-treated controls (Fig. 3i), indicating that this pathway might be targeted safely. Together, these data showed that sGPV specifically limited fibrin formation and pathological intravascular thrombus growth without impairing the initial platelet activation required for hemostasis.

Blocking GPV cleavage offsets defects in hemostatic platelet function

To further study thrombin interaction with GPV, we generated a panel of anti-GPV monoclonal antibodies (termed DOM monoclonal antibodies; Extended Data Fig. 7) and first evaluated their ability to inhibit thrombin-mediated GPV cleavage (Fig. 4a). Cleavage of substrates by thrombin involves binding and allosteric regulation by thrombin exosites I and II that flank the active site³⁸. Blockage of exosite I with the thrombin-binding aptamer HD1 (ref.³⁹) was more efficient

than blocking exosite II with HD22 (ref. 40), whereas a non-blocking aptamer HD23 had no effect on thrombin-mediated release of GPV from platelets (Extended Data Fig. 7g). Thus, thrombin interaction with fibrin and GPV occurred through overlapping sites³⁶. With this screening assay, we identified the monoclonal antibody DOM/B that markedly reduced thrombin-mediated GPV cleavage and synergized with thrombin exosite-directed aptamers (Fig. 4a and Extended Data Fig. 7g), whereas the monoclonal antibody DOM3 was non-inhibitory (Fig. 4a,f and Extended Data Fig. 7b). In PRP, we tested inhibitory activities of DOM/B in a thrombin-induced clotting assay, in which fibrin is formed independent of platelet activation. Whereas thrombin exosite II blockade with HD22 prolonged clotting times, clotting was unaffected by DOM/B treatment and was also indistinguishable between WT, *Gp5^{-/-}* and *Gp5^{dThr}* samples (Extended Data Fig. 7h). Thus, thrombin regulation by GPV specifically occurs under conditions of platelet activation under flow.

In addition, DOM/B had no effect on thrombin-induced platelet activation (Extended Data Fig. 7d–f), indicating that this monoclonal antibody did not sterically hinder the interaction of GPV with the GPIb–GPIX complex involved in GPIb α –thrombin–PAR platelet signaling. Remarkably, however, DOM/B significantly shortened time to fibrin formation and increased the amount of generated fibrin under flow conditions (Fig. 4b,c) as well as thrombin activity in the outflow of the flow chamber (Extended Data Fig. 8a), thereby reproducing the phenotypes seen with *Gp5^{-/-}* and *Gp5^{dThr}* mice. In line with reduced proteolytic release of GPV in the presence of DOM/B, we found less GPV colocalizing with fibrin than in controls (Extended Data Fig. 8b). The panel of anti-GPV monoclonal antibodies was also evaluated for interference with collagen-dependent platelet activation. Whereas DOM/B and DOM3 were non-inhibitory (Extended Data Fig. 7b,c), inhibition of platelet activation in this assay by DOM/C indicated that this monoclonal antibody was directed against the collagen-binding site of GPV (Extended Data Fig. 7a). DOM/C did not interfere with thrombin-mediated GPV cleavage (Fig. 4a) and did not enhance fibrin formation under flow, consistent with the crucial and specific role of sGPV release in this context (Fig. 4d,e). These data suggested that the collagen-binding activity of (s)GPV is functionally not required for its ability to modulate fibrin formation under flow in vitro and in vivo.

We next evaluated the effect of blocking GPV–thrombin interaction with DOM/B on fibrin and thrombus formation in vivo. Of note, injection of DOM/B did not cause platelet depletion and the monoclonal antibody remained detectable on the surface of circulating platelets for up to 6 d (Extended Data Fig. 8c,d). In line with the observed increased fibrin formation under flow in vitro, DOM/B treatment caused accelerated thrombus formation in FeCl₃-injured mesenteric

arterioles in vivo, whereas neither blockade of the collagen-binding site on GPV with DOM/C nor the non-inhibitory DOM3 affected thrombus formation (Fig. 4f,g). These data showed that the release of sGPV acts as a safety valve to limit thrombus growth after initial platelet activation required for hemostasis. We have previously shown that the absence of the two major collagen receptors GPVI and integrin $\alpha_2\beta_1$ causes severe bleeding in mice⁴¹. In line with the reversal of bleeding defects caused by GPVI deficiency in *Gp5^{-/-}* mice, DOM/B treatment restored hemostasis and thrombus formation in the complete absence of the two major platelet collagen receptors GPVI and $\alpha_2\beta_1$ (Extended Data Fig. 8e–g, summarized in Extended Data Fig. 8h).

These results suggest that interference with GPV cleavage can be used to enhance fibrin formation in the context of defective hemostasis caused by diverse mechanisms. We therefore investigated whether GPV-cleavage blockade with DOM/B not only restored hemostasis in the case of defective (hem)ITAM signaling but also other genetic and pharmacological impairments of platelet function. Lack of the small GTPase RhoA causes macrothrombocytopenia and defective platelet activation, resulting in a bleeding defect⁴². Similarly, neurobeachin-like 2 (NBEAL2) deficiency leads to macrothrombocytopenia and lack of α -granules, resulting in severely impaired hemostasis⁴³. Interestingly, DOM/B treatment improved and restored hemostasis in mice with platelet RhoA deficiency or lacking NBEAL2 (Fig. 4h,i).

Thrombocytopenia is a major clinical challenge occurring frequently in the context of a variety of pathologies or medical treatments that is associated with increased bleeding and often with the need for immediate therapeutic intervention^{44,45}. To test a possible benefit of a GPV-cleavage blockade in this setting, we induced severe thrombocytopenia by reducing platelet counts to 5–10% of normal by injecting a platelet-depleting antibody^{46,47}. While a resulting severe bleeding defect was observed in all nine platelet-depleted control mice, this was significantly attenuated by DOM/B treatment, and, remarkably, nine of 11 DOM/B-treated thrombocytopenic mice managed to stop bleeding within the observation period (Fig. 4j). The current clinical standard of care to reduce the risk of heart attack and ischemic stroke is the pharmacological inhibition of platelet function by purinergic P2Y₁₂ ADP receptor blockers alone or in combination with acetyl salicylic acid. As seen in humans, mice treated with the P2Y₁₂ blocker clopidogrel exhibited increased bleeding that was reversed by treatment with DOM/B, blocking thrombin-dependent GPV release from platelets (Fig. 4k). Thus, specific targeting of GPV with DOM/B prevented prolongation of the bleeding time caused by thrombocytopenia, genetic defects and anti-platelet therapy, indicating clinical potential of anti-GPV treatment to restore hemostasis by improving thrombin-dependent fibrin formation.

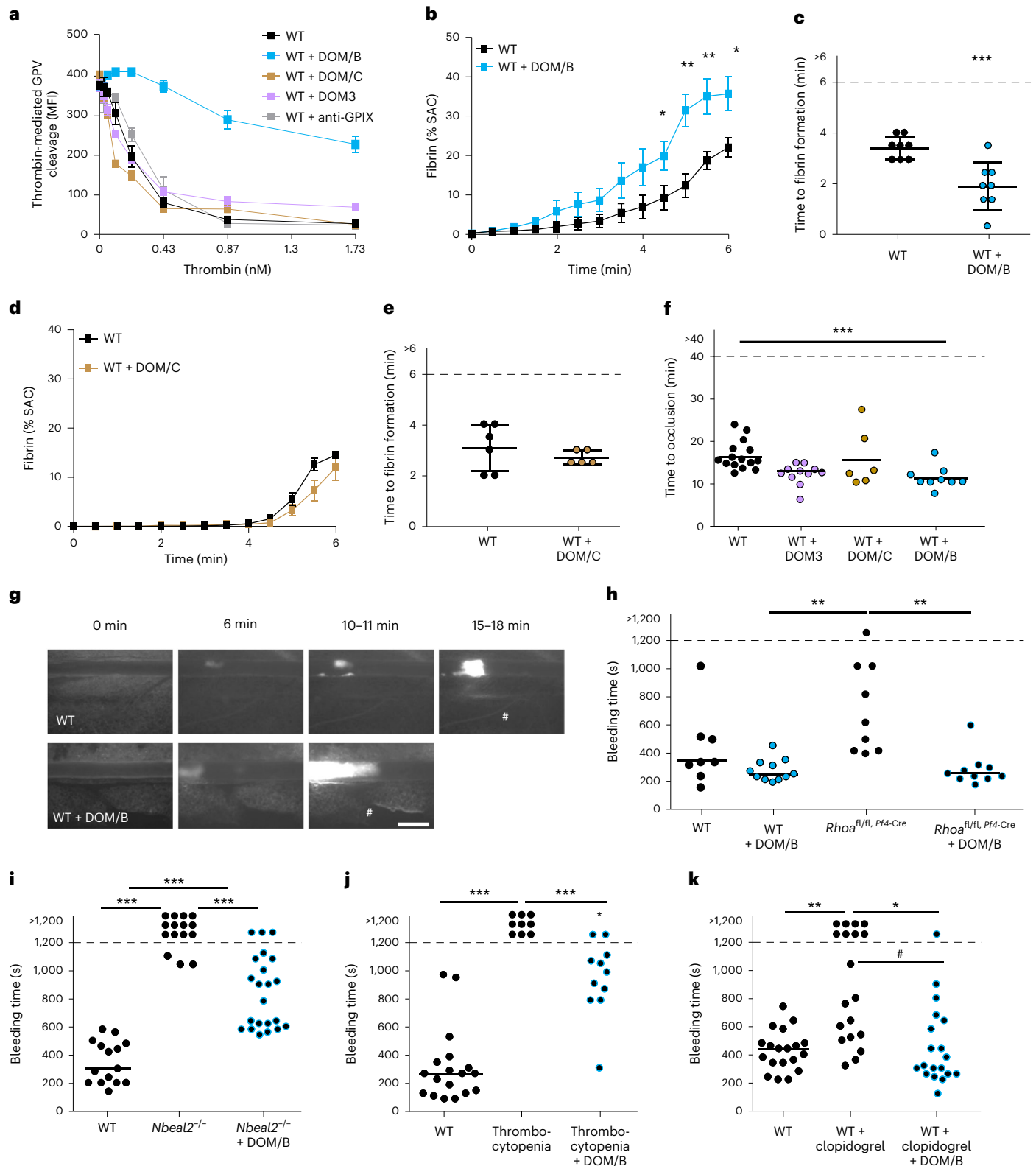
Fig. 4 | The anti-mGPV antibody DOM/B interferes with thrombin-mediated cleavage of GPV and reproduces the *Gp5^{-/-}* phenotype. **a**, Thrombin-mediated cleavage of GPV was assessed by flow cytometry. Mean \pm s.d., $n = 3$, four independent experiments. **b–e**, Recalcified whole blood was incubated in vitro with 10 $\mu\text{g ml}^{-1}$ anti-mGPV antibody before perfusion over collagen–TF spots. Quantification of fibrin generation during blood flow (**b,d**) and time to fibrin formation (**c,e**). **b**, Mean \pm s.e.m., $n = 8$, three independent experiments, two-tailed unpaired *t*-test with Welch's correction. *P* values: 4.5 min, $P = 0.0430$; 5 min, $P = 0.0029$; 5.5 min, $P = 0.0092$; 6 min, $P = 0.0186$. **c**, Mean \pm s.d., $n = 8$, four independent experiments, two-tailed unpaired *t*-test, $P = 0.0010$. **d**, Mean \pm s.e.m., $n = 3$, three independent experiments. **e**, Mean \pm s.d., three independent experiments, WT, $n = 6$; WT + DOM/C, $n = 5$. Quantification (**f**) and representative images (**g**) of thrombus formation upon FeCl₃-induced injury of mesenteric arterioles. WT (WT + control immunoglobulin (IgG)), $n = 15$ arterioles of eight mice; WT + DOM3, $n = 11$ arterioles of six mice; WT + DOM/C, $n = 6$ arterioles of four mice; WT + DOM/B, $n = 9$ arterioles of six mice. DOM/B versus WT, $P = 0.0008$. The symbol # indicates occlusive thrombus formation. Scale bar, 50 μm . **h–k**, Tail-bleeding time assays. **h**, WT (with control IgG), $n = 8$; WT + DOM/B, $n = 11$; *Rhoa*^{R/R, P/Δ-Cre}, $n = 9$; *Rhoa*^{R/R, P/Δ-Cre} + DOM/B, $n = 10$. *Rhoa*^{R/R, P/Δ-Cre} + DOM/B versus *Rhoa*^{R/R, P/Δ-Cre}, $P = 0.0064$; DOM/B versus *Rhoa*^{R/R, P/Δ-Cre},

$P = 0.002$. **i**, WT (with control IgG), $n = 15$; *Nbeal2^{-/-}*, $n = 15$; *Nbeal2^{-/-}* + DOM/B, $n = 22$. Open versus occluded vessels: WT versus *Nbeal2^{-/-}*, $P < 0.0001$; *Nbeal2^{-/-}* + DOM/B versus *Nbeal2^{-/-}*, $P < 0.0001$; comparison of occluded vessels: *Nbeal2^{-/-}* + DOM/B versus WT, $P < 0.0001$; WT versus *Nbeal2^{-/-}*, $P = 0.0006$. **j**, WT mice were injected with platelet-depletion antibody to induce thrombocytopenia (5–10% of normal counts). WT (with control IgG), $n = 18$; thrombocytopenia, $n = 9$; thrombocytopenia + DOM/B, $n = 11$; open versus occluded vessels: WT versus thrombocytopenic mice, $P < 0.0001$; thrombocytopenic mice + DOM/B versus thrombocytopenic mice, $P = 0.0003$; comparison of occluded vessels: thrombocytopenic mice + DOM/B versus WT, $P = 0.0251$. **k**, $n = 19$ (all groups). Open versus occluded vessels: WT versus WT + clopidogrel, $P = 0.0031$; WT + DOM/B + clopidogrel versus WT + clopidogrel, $P = 0.0188$; comparison of occluded vessels: WT + DOM/B + clopidogrel versus WT + clopidogrel, $^{\#}P = 0.0383$. **f, h–k**, Horizontal line represents mean. Horizontal dashed line in **c, e, f** and **h–k** indicates the end of the experiment; every dot above it did not show any occlusion/fibrin formation within the observation period. Two-tailed Kruskal–Wallis test followed by Dunn's multiple-comparison test to compare occluded vessels. Two-tailed Fisher's exact test was used to compare occluded versus non-occluded vessels. *, $P < 0.05$, **, $P < 0.01$, ***, $P < 0.001$.

Blocking GPV cleavage increases fibrin formation in human blood

We therefore evaluated the relevance of this concept for human platelet function and screened a panel of newly generated anti-human GPV (hGPV) monoclonal antibodies (termed LUM monoclonal antibodies) for their ability to interfere with thrombin-mediated cleavage of GPV. Recapitulating the inhibitory properties of DOM/B in the mouse system, LUM/B prevented thrombin-mediated cleavage of GPV on

human platelets, whereas other anti-hGPV monoclonal antibodies (LUM1–LUM5) were non-inhibitory (Fig. 5a and Extended Data Fig. 9c). LUM/B per se did not activate human platelets (Extended Data Fig. 9a,b) or influence thrombin clotting (Extended Data Fig. 9e) or thrombin-induced platelet activation as shown by unaltered integrin $\alpha_{IIb}\beta_3$ activation or P-selectin exposure in the presence of the antibody (Fig. 5b and Extended Data Fig. 9d). In the established flow assay on immobilized collagen–TF, GPV blockage on human platelets with LUM/B



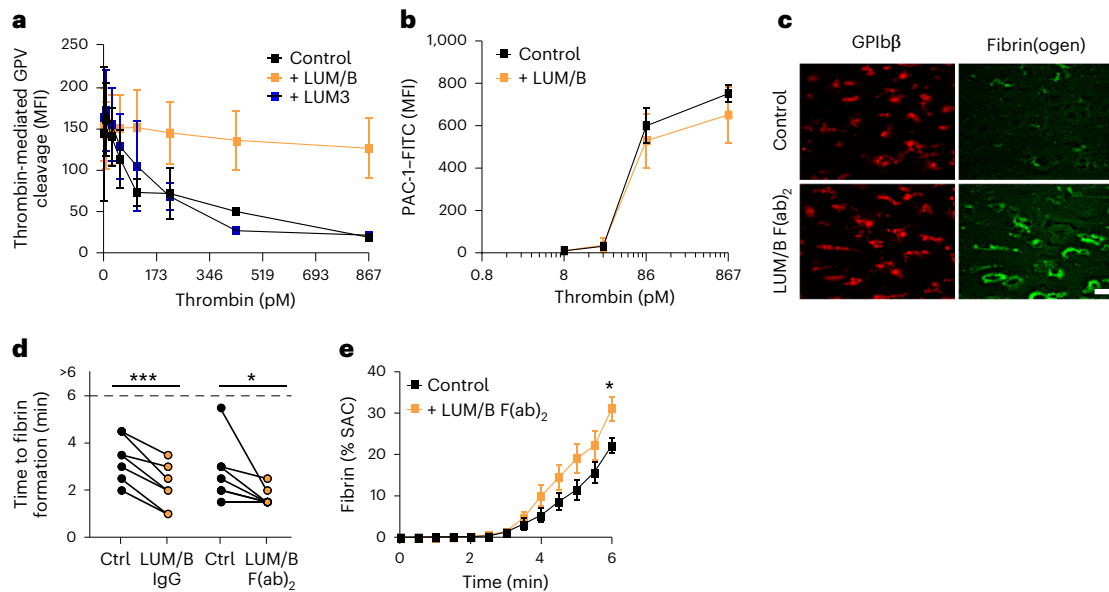


Fig. 5 | The anti-hGPV monoclonal antibody LUM/B interferes with thrombin cleavage and accelerates fibrin formation. **a**, Human platelets were incubated with the indicated antibody or control IgG ($10 \mu\text{g ml}^{-1}$) before thrombin stimulation. Thrombin-mediated cleavage of GPV was assessed by flow cytometry. Mean \pm s.d., $n = 4$ donors, three independent experiments. **b**, Flow cytometry reveals unaltered reactivity of LUM/B-treated platelets ($10 \mu\text{g ml}^{-1}$) upon thrombin stimulation compared to human controls. Mean \pm s.d., $n = 4$ donors, three independent experiments. **c–e**, Recalcified whole blood was incubated with LUM/B IgG or LUM/B F(ab)₂ before perfusion over collagen–TF spots. **c**, Representative images of thrombus (GPIIb/IIIa) and fibrin formation.

Scale bar, 20 μm . Quantification of time to fibrin formation (**d**) and fibrin generation during blood flow (**e**) after LUM/B treatment. **d**, Control (Ctrl) versus LUM/B IgG, $n = 7$, two-tailed paired t -test; control versus LUM/B F(ab)₂, $n = 7$, two-tailed Wilcoxon matched-pairs signed-rank test; control versus 1B1 IgG, $P = 0.006$; control versus 1B1 F(ab)₂, $P = 0.0313$. Horizontal dashed line indicates the end of the experiment; every dot above it did not show any occlusion/fibrin formation within the observation period. **e**, Mean \pm s.e.m. $n = 10$ donors, three independent experiments. Two-tailed unpaired t -test, 6 min, $P = 0.0159$. Control, human donor. * $P < 0.05$, ** $P < 0.01$, *** $P < 0.001$.

significantly accelerated fibrin formation in recalcified whole blood (Fig. 5c–e), whereas the non-inhibitory LUM3 antibody was without effect (Extended Data Fig. 9f,g). Thus, spatio-temporal control of fibrin formation on thrombogenic surfaces by GPV is a species-conserved mechanism to restrict thrombosis while preserving hemostasis.

Discussion

We here delineate the function of platelet GPV that is proteolytically released by thrombin in the context of platelet activation at sites of vascular injury. Genetic blockade of thrombin-mediated shedding of GPV uncovered the crucial role of sGPV as a regulator of fibrin formation and thrombus growth. The cleavage of membrane-bound GPV occurs after platelet adhesion and initiation of thrombin generation and is thus temporally separated from the initial hemostatic response. We show that generated sGPV then interacts with generated fibrin and dampens thrombin activity toward fibrinogen. This spatially restricted action of sGPV after release from the platelet surface specifically limits thrombus growth in vitro and in vivo (summarized in Fig. 6). As demonstrated by pharmacological application of rhGPV, sGPV provides protection from thrombo-inflammatory neurological damage in an experimental model of ischemic stroke without causing hemostatic impairments. Conversely, specific blockade of thrombin-mediated GPV shedding can enhance local fibrin formation in a variety of contexts associated with severe defects in platelet function. This unique spatio-temporal control of thrombin activity by GPV can thus be harnessed to promote hemostasis.

Prevention of thrombosis while preserving hemostasis has been a central goal of anti-thrombotic drug development. Despite the broader application and safety of target-selective oral anticoagulants, preventing bleeding complications remains an unmet clinical need. Although a recent study provides proof of principle that platelet-mediated thrombin generation can rescue bleeding defects due to increased

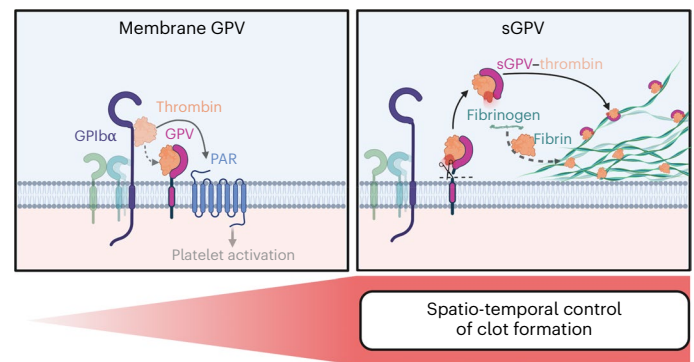


Fig. 6 | GPV modulates thrombin-mediated platelet activation and fibrin formation. On the platelet surface, GPV regulates platelet responsiveness to thrombin by interference with GPIIb/IIIa-dependent PAR signaling (left). Once GPV is cleaved by thrombin, sGPV dampens thrombin activity and fibrin formation, thereby controlling clot formation (right). Created with BioRender.

fibrinolysis⁴⁷, there is an unmet clinical need for more general and specific spatio-temporal control of fibrin formation. New hemostatic agents are approved or in development to bypass genetic or acquired deficiencies in the coagulation cascade⁴⁸, but platelet transfusion remains the only therapeutic option to acutely restore defective platelet function or severe forms of thrombocytopenia to secure hemostasis. Akin to the strategies that ‘inhibit the inhibitors’ of coagulation, we here propose a therapeutic strategy of tailored activation of hemostatic fibrin plug formation in the spatio-temporal context of platelet deposition at sites of vessel wall injury. By increasing local thrombin bioavailability without compromising scavenging of thrombin by endothelial cell-expressed thrombomodulin, this approach has little risk to interfere with physiological anticoagulation in the body and

vascular-protective and anti-inflammatory signaling of the protein C–PARI pathway¹⁰.

Methods

Animals

Mice were maintained under specific pathogen-free conditions (constant temperature of 20–24 °C and 45–65% humidity with a 12-h light–dark cycle, ad libitum water and food access), and experiments were performed in accordance with German law and the governmental bodies and with approval from the District of Lower Franconia.

Gp5^{−/−} (ref. ¹²) and *Itga2*^{−/−} (ref. ⁴⁹) mice were kindly provided by F. Lanza (Inserm-Université de Strasbourg, Strasbourg, France) and B. Eckes (Department of Dermatology, University of Cologne, Cologne, Germany), respectively. *Gp5*^{dtThr} mice, which carry a point mutation in the sequence corresponding to the thrombin cleavage site of GPV, were generated and are described in Extended Data Fig. 1a. *Gp5*^{dtThr} mice were intercrossed with Flip-positive mice to delete the Neo cassette and backcrossed to the C57Bl/6J background. *Rhoa*^{fl/fl} (ref. ⁵⁰) mice were kindly provided by C. Brakebusch (University of Copenhagen, Copenhagen, Denmark). To generate MK- or platelet-specific knockout mice, floxed mice were intercrossed with mice carrying the sequence for Cre recombinase under control of the *Pf4* (platelet factor) promoter. *Nbeal2*^{−/−} (ref. ⁴³) mice were described previously. All mice were kept on a C57Bl/6J background, and all animal experiments and analysis of the corresponding data were performed blinded.

Female Wistar rats (strain RjHan:WI, starting at 6 weeks of age) were immunized to generate monoclonal anti-GPV antibodies.

Human blood samples

For this study, blood samples were obtained from healthy volunteers, free from anticoagulant or anti-platelet therapy for at least 4 weeks, following written informed consent in accordance with the Declaration of Helsinki and after approval by the Institutional Review Boards of the University of Würzburg (votes 167/17 and 295/20).

Chemicals

Midazolam (Roche Pharma), dorbene (Pfizer) and fentanyl (Janssen-Cilag) were used according to regulations of the local authorities. Clopidogrel was from Sanofi, low-molecular-weight heparin was from ratiopharm, and recombinant hirudin was from CoaChrom. Human fibrinogen (F4883), bovine thrombin (T4648), *N*-ethylmaleimide (23030) and prostacyclin (PGI₂) were from Sigma-Aldrich. ProLong Glass Antifade Mountant (P36980) and fibrin(ogen) AF488 (F13191) were from Thermo Scientific. Iron(III) chloride (FeCl₃) was from Roth. A23187 was from AppliChem; ionomycin was from VWR. Convulxin was from Axxora. Fibrillar type I collagen (Horm) was from Takeda; rhodocytin was provided by J. Eble (University of Münster, Münster, Germany). Collagen-related peptide (CRP) was generated in house by formaldehyde cross-linking of GKO(GPO)₁₀GKOG (purchased from Cambridge Research Biochemicals, with O = L-hydroxyproline)⁵¹. Integrilin was from GlaxoSmithKline. Human thrombin was from Roche (Sigma-Aldrich, 10602400001). Apyrase type III was from GE Healthcare; biotinylated thrombin (69672-3) was from Merck-Millipore. Z-GGR-AMC-HCl was from Bachem; thrombin calibrator was from Stago; human recombinant TF (Dade Innovin) was from Siemens Healthcare. The fluorogenic thrombin substrate Pefluor TH was from Pentapharm. Donkey anti-rat IgG FITC (112095068) was from Jackson ImmunoResearch. DNA aptamers (HD1, GGTTGGTGTGGTTGG; HD22, AGTCCGTGGTAGGGCAGGTTGGGGTGACT) to block thrombin exosites and the control aptamer HD23 (AGTCCGTAATAAGCAGGTTAAAT-GACT) were from Future Synthesis.

Antibodies

PAC-1-FITC (340507) and anti-CD62P-APC (550888) antibodies were from BD Biosciences; control rat IgG (14131) and anti-GAPDH antibody

(G9545) were from Sigma. Anti-mGPV antibody (AF6990) for western blot analysis was from R&D; the anti-hGPV antibody (sc271662) for western blot analysis was from Santa Cruz. The platelet-depletion antibody R300 (rat anti-GPIb α IgG antibody) was from Emfret Analytics. Anti-mCD31 antibody (clone 390, conjugated in house to AF647) was from BioLegend (102402). A detailed list of antibodies generated in house is provided in Supplementary Table 1 (refs. ^{52–62}).

New antibodies were generated by hybridoma technology following immunization of *Gp5*^{−/−} mice or Wistar rats with recombinant hGPV protein or GPV immunoprecipitated from mouse or human platelet lysates.

Expression and purification of recombinant hGPV

The gene fragment encoding the GP64 signal peptide (MVSIV-LYVLLAAAHSFAFA), the human GPV extracellular domain (amino acids 17–518) and a decahistidine tag was amplified, inserted into the pFastBac dual vector and transformed into the DH10Bac *Escherichia coli* strain (Thermo Fisher Scientific). The resulting bacmid DNA was prepared and then transfected into Sf9 insect cells (Thermo Fisher Scientific, 11496015) using CellFectin II reagent (Thermo Fisher). The high-titer P2 baculovirus stock was prepared from scaled-up Sf9 cells in Sf-900 II serum-free medium (Thermo Fisher Scientific, 10902088) following the instructions for the Bac-to-Bac Baculovirus Expression System (Thermo Fisher Scientific) and used to induce hGPV expression in Sf9 cells (2×10^6 cells per ml, MOI of 2) for 72 h. hGPV was purified from insect cell medium by Ni affinity chromatography using a GE Healthcare Ni Sepharose excel column (elution buffer: 20 mM sodium phosphate, 500 mM NaCl, 500 mM imidazole, pH 7.4), followed by size-exclusion chromatography using a GE Healthcare HiLoad 16/600 Superdex 200-pg column (elution buffer: PBS containing 0.1% Tween-20, pH 7.4). The purified protein was stored at −80 °C in PBS containing 0.1% Tween-20 and 20% glycerol. Notably, rhGPV precipitated at concentrations above 0.5 mg ml^{−1}, limiting its biophysical characterization.

Antibody treatment

For antibody treatment experiments, mice were separated into antibody and control treatment groups in a randomized manner using <https://www.random.org/lists/>. Next, 100 μ g JAQ1 IgG was injected intraperitoneally at day 7 and day 5 before the experiment, resulting in a GPVI-knockout-like phenotype³¹. All other antibodies (each 100 μ g) were injected i.v. or i.p. directly before the experiment.

Platelet depletion

Thrombocytopenia was induced by intravenous injection of the rat anti-GPIb α IgG antibody R300 (Emfret Analytics, 0.14–0.18 μ g per g body weight). This low dose of platelet-depletion antibody reduced the platelet count to 5–10% of the initial platelet count⁴⁶. Peripheral platelet count was determined by flow cytometry 16 h after platelet depletion (before the tail-bleeding time experiment).

Treatment with clopidogrel or rhGPV

Mice were fed orally with 3 mg per kg clopidogrel 48 h and 24 h before the experiment. A dose titration for rhGPV was performed using 10–80 μ g rhGPV per mouse in an arterial thrombosis model. The dose of 10 μ g rhGPV resulted in variable results, while no difference in the anti-thrombotic effect of rhGPV was noted for 20, 40 or 80 μ g rhGPV per mouse. Consequently, 20 μ g (as the lowest rhGPV concentration that yielded reproducible results) was chosen for all in vivo experiments, and 20 μ g ml^{−1} was chosen for in vitro assays. Mice were injected intravenously with 20 μ g rhGPV 5 min before the experiment.

Preparation of PRP and washed platelets

Mice were anesthetized using isoflurane and bled to 300 μ l heparin (20 U ml^{−1} in TBS, pH 7.3, ratiopharm). The blood was centrifuged twice at 300g for 6 min to obtain PRP. PRP was supplemented with

0.02 U ml⁻¹ apyrase (A610, Sigma-Aldrich) and 0.1 µg ml⁻¹ PGI₂ (P6188, Sigma-Aldrich), and platelets were pelleted by centrifugation at 800g for 5 min and washed twice with Tyrode's buffer (134 mM NaCl, 0.34 mM Na₂HPO₄, 2.9 mM KCl, 12 mM NaHCO₃, 5 mM HEPES, 5 mM glucose, 0.35% BSA, pH 7.4) containing 0.02 U ml⁻¹ apyrase and 0.1 µg ml⁻¹ PGI₂. The platelets were allowed to rest for at least 30 min at 37 °C before experiments.

Aggregation assay

Washed platelets (160 µl with 1.5 × 10⁵ platelets per µl) and PRP (only used for ADP stimulation) were prepared as described. For aggregometry, washed platelets were analyzed in the absence (thrombin) or presence (all other agonists) of 70 µg ml⁻¹ human fibrinogen. Antibodies (10 µg ml⁻¹) were pre-incubated for 5 min at 37 °C before the experiment. Light transmission was recorded on a four-channel aggregometer (Fibrintimer, APACT) for 10 or 20 min (in the presence of LEN/B) and expressed in arbitrary units, with buffer representing 100% light transmission. Platelet aggregation was induced by addition of the indicated agonists.

Flow cytometry

To determine glycoprotein surface expression levels, whole blood was diluted 1:20 with Ca²⁺-free Tyrode's buffer or PBS and stained with saturating amounts of fluorophore-conjugated antibodies for 15 min at room temperature in the dark.

Washed platelets adjusted to 50,000 per µl in Tyrode's buffer with Ca²⁺ were stimulated with the indicated agonists and incubated with saturating amounts of fluorophore-conjugated antibodies to determine platelet activation or thrombin-mediated cleavage of GPV. Human thrombin (Sigma, 10602400001) was used to stimulate platelets.

All samples were analyzed directly after addition of 500 µl PBS on a FACSCalibur (BD Biosciences) using CellQuest Pro (version 6.0) software. Data were analyzed using FlowJo (version 10.7 and version 10.8.1). An exemplified gating strategy based on FSC-SSC characteristics is provided in Supplementary Fig. 2.

Thrombin- and *N*-ethylmaleimide-induced cleavage of GPV

Washed platelets were adjusted to a concentration of 1 × 10⁶ platelets per µl in Tyrode's buffer without Ca²⁺ and diluted 1:1 with Tyrode's buffer without Ca²⁺ (for resting and thrombin-stimulated samples (human thrombin (Sigma, 10602400001))) and with Tyrode's buffer with Ca²⁺ (for *N*-ethylmaleimide (2 mM final concentration (f.c.))-incubated samples). Stimulation with 867 pM thrombin (for human thrombin, 0.1 U ml⁻¹ is equivalent to 867 pM thrombin) for 30 min at 37 °C was performed in the presence of 40 µg ml⁻¹ integrilin and 5 µM EGTA to prevent platelet aggregation. Afterwards, the platelet suspension was diluted, incubated with saturating amounts of FITC-conjugated platelet surface antibodies and directly analyzed on a FACSCalibur. The residual platelet suspension was pelleted, and the supernatant was analyzed in an ELISA for GPV.

GPV enzyme-linked immunosorbent assay

Ninety-six-well plates (Hartenstein, F-form) were coated with 50 µl per well DOM/C antibody (30 µg ml⁻¹) in carbonate buffer overnight at 4 °C, blocked with 5% non-fat dried milk in PBS for 2 h at 37 °C and washed. Samples were applied to plates, incubated for 1 h at 37 °C and washed. Plates were incubated with HRP-labeled DOM/B antibody for 1 h and washed again three times, and samples were developed using TMB substrate. The reaction was stopped by addition of 0.5 M H₂SO₄. Optical density was measured on a Multiskan EX device (Thermo Electron). Absorbance was read at 450 nm; the 620-nm filter served as the reference wavelength. Plasma samples from *Gp5^{-/-}* mice served as the negative control; supernatant after platelet thrombin stimulation served as the positive control.

Clot retraction

Clot-retraction studies were performed at 37 °C in an aggregometer tube containing diluted PRP (3 × 10⁵ platelets per µl), thrombin (34.68 nM) and CaCl₂ (20 mM). Clot retraction was recorded with a camera over a time span of 2 h after activation.

Thrombin time

To determine thrombin time, citrated PRP was diluted 1:1 in PBS and stimulated with 17.5 nM f.c. bovine thrombin (equivalent to 2 U ml⁻¹). Thrombin time was analyzed with a four-channel mechanical ball coagulometer (Merlin Medical).

Thrombin generation

Thrombin generation was quantified in recalcified citrate anticoagulated PRP with platelet count adjusted to 1.5 × 10⁵ platelets per µl. Platelets were resuspended in pooled plasma preparations from two to four mice with the same genotype. After platelet stimulation with the indicated agonists (15 min at 37 °C), samples in duplicates (four volumes) were transferred to a polystyrene Immulon 2HB 96-well plate. The wells either contained one volume thrombin calibrator or TF (1 pM f.c.). Coagulation was initiated by adding one volume of fluorescent thrombin substrate (2.5 mM Z-GGR-AMC). Thrombin generation was measured and analyzed using Thrombinoscope software (version 5.0.0.742, Thrombinoscope)^{63,64}.

Static fibrin polymerization

Unlabeled fibrinogen (1.35 mg ml⁻¹ f.c.) and AF488-labeled fibrinogen (45 µg ml⁻¹ f.c.) were mixed (30:1) in the absence or presence of rhGPV (20 µg ml⁻¹, stained with LUM/B AF647). Fibrin polymerization was initiated by addition of 867 pM thrombin or 1 U ml⁻¹ batroxobin (Loxo) in the presence of 5 mM CaCl₂. The mixture was immediately transferred to an uncoated eight-well 15µ-slide (ibidi), which was placed in a dark humidity chamber for 2 h at room temperature to allow fibrin polymerization. Images were obtained using a Leica SP8 inverted microscope with a ×63 oil-immersion lens. Optical z stacks (8 µm, step size of 0.1, Nyquist conform) were deconvolved (Huygens Essential software, version 21.04) and are shown as a maximum projection (ImageJ software). Fibrin fibers per visual field and surface coverage of hGPV staining were quantified using Fiji.

Coagulation flow chamber

Glass coverslips were coated with collagen type I (10 µl, 50 µg ml⁻¹) and TF (10 µl, 100 pM or 10 pM) for experiments with human blood or mouse blood, respectively) and blocked with 1% BSA-PBS. Citrated whole blood was recalcified by co-infusion with 6.3 mM CaCl₂ (f.c.) and 3.2 mM MgCl₂ (f.c.) and perfused over the collagen-TF spots for up to 6 min at a shear rate of 1,000 s⁻¹ (ref. ⁶⁵). Before each experiment, blood samples were pre-labeled with AF488-conjugated fibrinogen, an anti-GPIX derivative (mouse) or an anti-GPIIb derivative (human) to stain platelets. For human samples, control and antibody-treated samples of the same donor were always run in parallel.

Time series experiments. Before each experiment, blood samples were pre-incubated with AF488-conjugated fibrinogen, AF647-conjugated anti-GPIX derivative (mouse) or AF647-conjugated anti-GPIIb derivative (human) platelets. For time series experiments, fluorescence microscopic images were captured at 30-s intervals to evaluate kinetics for up to 6 min (Leica DMI 6000 B, ×63 objective, Leica Application Suite (LAS) X software (version 1.9.013747)). Recorded images were further processed with the background-subtraction method Instant Computational Clearing) to remove out-of-focus blur on a Leica THUNDER microscope (LAS X software version 3.7). Next, the exported images were analyzed for surface area coverage of fibrin formation with self-written Python scripts⁶⁶. In detail, in the first step, an entropy filter with a disk size of five pixels was applied, followed by a median

filter (disk size, ten pixels) and Otsu thresholding. To compensate for a nearly empty field of view during the first images in the time series, we introduced a ‘scaling factor’, sf , with which we multiplied the found Otsu threshold value and thus increased the threshold slightly for the first images (usually the first 60–150 s, with $sf = 1.03$ – 1.05). The thresholded area (as a fraction of the whole field of view) represents the area covered by fibrin.

For heatmap representation, mean values were univariate scaled from -4 to 4 . Gene effect heatmaps were constructed by subtracting scaled average values of the control strain from those of the mutant strain. For details, see ref.³⁵.

Three-dimensional confocal microscopy. Samples were stained as described for Time series experiments. To acquire zstacks of complete thrombi, samples were fixed with 4% paraformaldehyde (PFA)–PBS, mounted with ProLong Glass (Thermo Scientific) and further analyzed by confocal microscopy (Leica SP8 inverted microscope). z stacks of thrombi were acquired with an SP8 confocal microscope (Leica) in HyVolution mode ($\times 63$; z step, $0.1 \mu\text{m}$). Images were deconvolved using Huygens Professional software (version 21.04) with a signal-to-noise ratio between 2 and 10 (identical for regions of interest in the same animal), an automatic background subtraction using the ‘in/near object’ option with a search radius of $2 \mu\text{m}$ and a maximum of 40 iterations. The deconvolved dataset was exported in Imaris file format and visualized with Fiji⁶⁷ (<https://www.biovoxxel.de/development/>).

To analyze GPV–fibrin localization outside the thrombus, blood samples were pre-incubated with AF488-conjugated fibrinogen, AF546-conjugated anti-GPV derivative (as direct labeling of rhGPV with a fluorophore abolished its biological activity) and AF405-conjugated anti-GPIX derivative. Single images from the bottom of a thrombus were acquired using a Zeiss LSM 980 Airyscan microscope ($\times 63$ objective) in super-resolution mode using the smart setup. Images were deconvolved with Zeiss ZEN software (version 3.2) and analyzed with Fiji. First, masks from the fibrin(ogen) and platelet (GPIX) channels were generated using Li thresholding. Masks were then used as ‘positive’ (pixel intensity of 1 inside the structure and 0 outside the structure) and ‘negative’ (pixel intensity of 0 inside the structure and 1 outside the structure) imprints and applied to the GPV channel. To analyze GPV intensities outside the thrombus but inside fibrin fibers, the positive fibrin mask was multiplied with the negative thrombus mask.

In detail, after Li thresholding, the intensity values in the binarized images were changed to 0 and 1 by dividing through 255. Next, this procedure for preparation of the positive and negative binary masks was repeated for the GPIX channel. Afterward, the prepared masks based on single-channel thresholds were combined by multiplication (leading to a value of 1 if positive in both masks). This resulted in the following regions: (1) inside fibrin but non-platelet area and (2) outside fibrin and non-platelet area \rightarrow background count rate.

Finally, the intensity of GPV was determined in the area of fibrin by multiplication of the obtained masks with the GPV channel. Values outside the mask were set to 0, and pixels inside the mask have an intensity of 1, thus the original intensity of GPV was preserved. This calculation was performed for all masks, and surface coverage as well as raw integrated density were determined. Next, the average intensity per pixel was calculated inside the covered area, and the raw integrated density was divided by the number of pixels to obtain the average intensity per non-zero pixel.

For each step, a Fiji macro was recorded. All Fiji macros and Python scripts used for fluorescence image analysis can be downloaded from <https://github.com/HeinzeLab/GPV-flowchamber>.

Thrombin activity

The coagulation flow assay was performed as described above without staining for platelets and fibrin(ogen). The outflow was collected in

10 mM EDTA and $1.5 \mu\text{M}$ HD1. Thrombin activity was measured immediately using the fluorogenic thrombin substrate Pefaflo TH (Pentapharm) at 460 nm.

Thrombin activity in the formed thrombi was determined using the fluorogenic thrombin substrate Z-GGR-AMC.

Western blot after pulldown

Washed platelets were adjusted to 1×10^6 platelets per μl and either left unstimulated or were stimulated with biotinylated thrombin (433 pM) for 15 min at 37°C . When indicated, hirudin (0.1 U ml^{-1}) or GM6001 ($100 \mu\text{M f.c.}$) was added before platelet stimulation. Platelets were pelleted, and the supernatant was incubated with magnetic streptavidin beads to pull down biotinylated thrombin. After incubation, beads were collected and washed. The eluate was used for western blot analysis, and the samples were detected with an anti-GPV antibody (R&D).

GPV–thrombin interaction in solution

We performed cross-linking experiments with BS3 or DTSSP following incubation of thrombin with varying concentrations of rhGPV. However, conditions with efficient cross-linking could not be established. Thrombin interaction with rhGPV was furthermore analyzed in a solution (HEPES buffer), and generation of sGPV was followed by western blotting and detection with an anti-hGPV antibody (Santa Cruz, sc271662). A serial dilution of cleaved sGPV was used to quantify the reaction product. The stability of thrombin was analyzed under the same conditions by determining thrombin activity with the chromogenic substrate S2238 (Chromogenix).

Tail-bleeding time

Mice were anesthetized by intraperitoneal injection of triple anesthesia (Dormitor, $0.5 \mu\text{g per g}$; midazolam, $5 \mu\text{g per g}$; and fentanyl, $0.05 \mu\text{g per g}$ body weight), and a 1-mm segment of the tail tip was removed using a scalpel. Tail bleeding was monitored by gently absorbing blood on filter paper at 20-s intervals without directly contacting the wound site. When no blood was observed on the paper, bleeding was determined to have ceased. The experiment was manually stopped after 20 min by cauterization.

Light sheet fluorescence microscopy

Sample preparation. The vasculature was stained by intravenous injection of AF647-conjugated anti-CD105 (clone MJ7/19, purified in house, $0.4 \mu\text{g per g}$ body weight) and AF647-conjugated anti-CD31 (BioLegend, clone 390, $0.4 \mu\text{g per g}$ body weight) antibodies. After in vivo labeling (30 min), mice were anesthetized by intraperitoneal injection of medetomidine ($0.5 \mu\text{g per g}$ body weight), midazolam ($5 \mu\text{g per g}$ body weight) and fentanyl ($0.05 \mu\text{g per g}$ body weight) and transcardially perfused with ice-cold PBS to wash out the blood and ice-cold 4% PFA (P6148, Sigma-Aldrich, pH 7.2). Brains were removed, washed with PBS and dehydrated in methanol solutions of increasing concentrations (50%, 70%, 95%, 100%) to fix the tissue. The methanol was replaced stepwise by a clearing solution consisting of one part benzyl alcohol to two parts benzyl benzoate (BABB; 305197 and B6630, Sigma-Aldrich). After incubation in the clearing solution for at least 2 h at room temperature, tissue specimens became optically transparent and were used for light sheet fluorescence microscopy (LSFM) imaging on the following day⁶⁸.

Optically cleared brains were imaged with a custom-built light sheet microscope equipped with two EC Epiplan Neofluar $\times 2.5/0.06$ M27 excitation objectives (Zeiss) and an HCX Fluotar $\times 5/0.15$ dry detection objective (Leica)²⁹ with a voxel size of $2.6 \mu\text{m}$ and z spacing of $5 \mu\text{m}$ (pixel size, $2.6 \times 2.6 \times 5 \mu\text{m}$). Major parts of the LSFMs have been described previously⁶⁹. Additionally to the fluorescence signal of the AF647-conjugated antibodies staining the vessel system, brain autofluorescence was also collected by excitation at 488 nm with emission at 520 nm.

Segmentation of brain LSFM images

Images acquired by LSFM were saved in TIFF format and converted to the Imaris file format (Imaris 9.9, Bitplane, Oxford) for further processing and segmentation. Using the built-in image-processing tools, first the background was subtracted from both channels, and secondly a $3 \times 3 \times 3$ -voxel median filter was applied to the vessel channel (AF647 fluorescence). Next, the median-filtered vessel channel was segmented using the surface tool. Here, four-voxel smoothing (10.4 μm) and local contrast intensity thresholding (10 μm in diameter) were applied. The intensity threshold was adjusted manually to ~50% of the automatically proposed value. Finally, objects smaller than 1,000 voxels were removed.

Determination of vessel diameter

To determine the diameter of the vessel at selected regions of interest, the generated vessel surface was masked onto the vessel fluorescence such that the intensity outside the surface was zero, while, inside the surface, the original, median-filtered intensity values were present.

To estimate the diameter, the ‘measurement points’ option in Imaris was used, which was placed directly on the border of the selected vessel regions of interest. Correct placing of the measurement points was ensured by 3D inspection of the images.

Transient middle cerebral artery occlusion

Focal cerebral ischemia was induced by tMCAO as previously described⁷⁰. Briefly, a silicon-coated thread was advanced through the carotid artery up to the origin of the MCA, causing an MCA infarction. After an occlusion time of 60 min, the filament was removed, allowing reperfusion of the MCA territory. The extent of edema corrected brain infarction was quantitatively assessed 24 h after reperfusion on 2,3,5-triphenyltetrazolium chloride-stained consecutive brain sections. Neurological function was analyzed by calculating a neuroscore (score, 0–10) based on the direct sum of the Grip test (score, 0–5) and the inverted Bederson score (score, 0–5).

Posterior communicating artery scores

Posterior communicating artery (PcomA) scores were determined in brains from mice that were perfused with PBS followed by 3 ml black ink diluted in 4% PFA (1:5, vol/vol).

Mechanical injury of the abdominal aorta

To open the abdominal cavity of anesthetized mice (8–20 weeks old), a longitudinal midline incision was performed, and the abdominal aorta was exposed. A Doppler ultrasonic flow probe (0.5PSB699, Transonic Systems) was placed around the vessel, and thrombus formation was induced by a single firm compression (20 s) with a forceps upstream of the flow probe. Blood flow was monitored over 30 min or until complete occlusion occurred (blood flow stopped for >5 min). The abdominal aorta was excised and embedded in Tissue-Tek. Sections (5 μm) were fixed and stained according to the Carstairs method to distinguish platelets and fibrin⁷¹. Images of Carstairs stained sections were acquired on a Leica DMI400B using LAS software (version 2.6.0.R1).

FeCl₃-induced injury of mesenteric arterioles

Four-week-old mice were anesthetized, and the mesentery was exteriorized. Arterioles (35–60 μm in diameter) were visualized with a Zeiss Axiovert 200 inverted microscope ($\times 10/0.25$ air objective) equipped with a 100-W HBO mercury lamp and a CoolSNAP EZ camera (Visitron) using MetaMorph software (version 6.2r6). Endothelial injury was induced by topical application of a 3-mm² filter paper saturated with ferric chloride (FeCl₃; 20%). Adhesion and aggregation of fluorescently labeled platelets (DyLight 488-conjugated anti-GPIX derivative) were monitored for 40 min or until complete occlusion occurred (blood flow stopped for >1 min).

Data analysis

The presented results are mean \pm s.d. from three independent experiments per group, and lines represent mean values, if not stated otherwise. Normal distribution was tested using the Shapiro–Wilk normality test. If passed, *P* values were calculated using the two-tailed unpaired *t*-test (two groups); if the values were not normally distributed, differences between two groups were analyzed using the Mann–Whitney two-tailed test. For more than two groups, one-way ANOVA (Kruskal–Wallis test) followed by Dunn’s test for multiple comparisons was performed using GraphPad Prism software (versions 7.03 and 7.05.). Two-tailed paired *t*-test (two groups, normally distributed), Wilcoxon matched-pairs signed-rank test (two groups, not normally distributed) and Friedman test followed by Dunn’s test for multiple comparisons (more than two groups, not normally distributed) were used for paired comparisons. For statistical analysis of non-occluded versus occluded vessels, Fisher’s exact *t*-test was used. *P* values < 0.05 were considered statistically significant.

Reporting summary

Further information on research design is available in the Nature Portfolio Reporting Summary linked to this article.

Data availability

All data supporting the analyses presented in this study are provided in the text and its associated files.

Code availability

Macros used for quantitative image analysis are available at <https://github.com/HeinzelLab/GPV-flowchamber>.

References

- Swieringa, F., Spronk, H. M. H., Heemskerk, J. W. M. & van der Meijden, P. E. J. Integrating platelet and coagulation activation in fibrin clot formation. *Res. Pract. Thromb. Haemost.* **2**, 450–460 (2018).
- Furie, B. & Furie, B. C. The molecular basis of blood coagulation. *Cell* **53**, 505–518 (1988).
- Tomaiuolo, M., Brass, L. F. & Stalker, T. J. Regulation of platelet activation and coagulation and its role in vascular injury and arterial thrombosis. *Interv. Cardiol. Clin.* **6**, 1–12 (2017).
- Kahn, M. L. et al. A dual thrombin receptor system for platelet activation. *Nature* **394**, 690–694 (1998).
- Stalker, T. J. et al. Hierarchical organization in the hemostatic response and its relationship to the platelet-signaling network. *Blood* **121**, 1875–1885 (2013).
- Versteeg, H. H., Heemskerk, J. W., Levi, M. & Reitsma, P. H. New fundamentals in hemostasis. *Physiol. Rev.* **93**, 327–358 (2013).
- Sang, Y., Roest, M., de Laat, B., de Groot, P. G. & Huskens, D. Interplay between platelets and coagulation. *Blood Rev.* **46**, 100733 (2021).
- Silva, L. M. et al. Fibrin is a critical regulator of neutrophil effector function at the oral mucosal barrier. *Science* **374**, eabl5450 (2021).
- Ryu, J. K. et al. Fibrin-targeting immunotherapy protects against neuroinflammation and neurodegeneration. *Nat. Immunol.* **19**, 1212–1223 (2018).
- Mosnier, L. O., Zlokovic, B. V. & Griffin, J. H. The cytoprotective protein C pathway. *Blood* **109**, 3161–3172 (2006).
- Ruggeri, Z. M. et al. Unravelling the mechanism and significance of thrombin binding to platelet glycoprotein Ib. *Thromb. Haemost.* **104**, 894–902 (2010).
- Kahn, M. L. et al. Glycoprotein V-deficient platelets have undiminished thrombin responsiveness and do not exhibit a Bernard–Soulier phenotype. *Blood* **94**, 4112–4121 (1999).
- Li, R. & Emsley, J. The organizing principle of the platelet glycoprotein Ib–IX–V complex. *J. Thromb. Haemost.* **11**, 605–614 (2013).

14. Mo, X., Liu, L., Lopez, J. A. & Li, R. Transmembrane domains are critical to the interaction between platelet glycoprotein V and glycoprotein Ib-IX complex. *J. Thromb. Haemost.* **10**, 1875–1886 (2012).
15. Moog, S. et al. Platelet glycoprotein V binds to collagen and participates in platelet adhesion and aggregation. *Blood* **98**, 1038–1046 (2001).
16. Nieswandt, B. & Watson, S. P. Platelet-collagen interaction: is GPIIb/IIIa the central receptor? *Blood* **102**, 449–461 (2003).
17. Clemetson, K. J. A short history of platelet glycoprotein Ib complex. *Thromb. Haemost.* **98**, 63–68 (2007).
18. Katsutani, S. et al. Cloning and characterization of the gene encoding the murine glycoprotein V: the conserved thrombin-cleavable protein on platelet surface. *Thromb. Res.* **92**, 43–51 (1998).
19. Ravanat, C. et al. Gene cloning of rat and mouse platelet glycoprotein V: identification of megakaryocyte-specific promoters and demonstration of functional thrombin cleavage. *Blood* **89**, 3253–3262 (1997).
20. Ni, H. Increased thrombogenesis and embolus formation in mice lacking glycoprotein V. *Blood* **98**, 368–373 (2001).
21. Rabie, T., Strehl, A., Ludwig, A. & Nieswandt, B. Evidence for a role of ADAM17 (TACE) in the regulation of platelet glycoprotein V. *J. Biol. Chem.* **280**, 14462–14468 (2005).
22. Ramakrishnan, V. et al. Increased thrombin responsiveness in platelets from mice lacking glycoprotein V. *Proc. Natl Acad. Sci. USA* **96**, 13336–13341 (1999).
23. Nonne, C., Hechler, B., Cazenave, J. P., Gachet, C. & Lanza, F. Reassessment of in vivo thrombus formation in glycoprotein V deficient mice backcrossed on a C57Bl/6 strain. *J. Thromb. Haemost.* **6**, 210–212 (2008).
24. McGowan, E. B., Ding, A. & Detwiler, T. C. Correlation of thrombin-induced glycoprotein V hydrolysis and platelet activation. *J. Biol. Chem.* **258**, 11243–11248 (1983).
25. Estevez, B. et al. Signaling-mediated cooperativity between glycoprotein Ib-IX and protease-activated receptors in thrombin-induced platelet activation. *Blood* **127**, 626–636 (2016).
26. Celikel, R. et al. Modulation of α -thrombin function by distinct interactions with platelet glycoprotein Iba. *Science* **301**, 218–221 (2003).
27. Dumas, J. J., Kumar, R., Seehra, J., Somers, W. S. & Mosyak, L. Crystal structure of the GpIb α -thrombin complex essential for platelet aggregation. *Science* **301**, 222–226 (2003).
28. Massberg, S. et al. A crucial role of glycoprotein VI for platelet recruitment to the injured arterial wall in vivo. *J. Exp. Med.* **197**, 41–49 (2003).
29. Stegner, D. et al. Foudroyant cerebral venous (sinus) thrombosis triggered through CLEC-2 and GPIIb/IIIa dependent platelet activation. *Nat. Cardiovasc. Res.* **1**, 132–141 (2022).
30. Bender, M. et al. Combined in vivo depletion of glycoprotein VI and C-type lectin-like receptor 2 severely compromises hemostasis and abrogates arterial thrombosis in mice. *Arterioscler. Thromb. Vasc. Biol.* **33**, 926–934 (2013).
31. Nieswandt, B. et al. Long-term antithrombotic protection by in vivo depletion of platelet glycoprotein VI in mice. *J. Exp. Med.* **193**, 459–469 (2001).
32. Mangin, P. et al. Thrombin overcomes the thrombosis defect associated with platelet GPIIb/IIIa deficiency. *Blood* **107**, 4346–4353 (2006).
33. Mangin, P. H. et al. Immobilized fibrinogen activates human platelets through glycoprotein VI. *Haematologica* **103**, 898–907 (2018).
34. de Witt, S. M. et al. Identification of platelet function defects by multi-parameter assessment of thrombus formation. *Nat. Commun.* **5**, 4257 (2014).
35. Nagy, M. et al. Comparative analysis of microfluidics thrombus formation in multiple genetically modified mice: link to thrombosis and hemostasis. *Front. Cardiovasc. Med.* **6**, 99 (2019).
36. Fredenburgh, J. C., Stafford, A. R., Leslie, B. A. & Weitz, J. I. Bivalent binding to γ A/ γ '-fibrin engages both exosites of thrombin and protects it from inhibition by the antithrombin-heparin complex. *J. Biol. Chem.* **283**, 2470–2477 (2008).
37. Stoll, G. & Nieswandt, B. Thrombo-inflammation in acute ischaemic stroke—implications for treatment. *Nat. Rev. Neurol.* **15**, 473–481 (2019).
38. Petrer, N. S. et al. Long range communication between exosites 1 and 2 modulates thrombin function. *J. Biol. Chem.* **284**, 25620–25629 (2009).
39. Bock, L. C., Griffin, L. C., Latham, J. A., Vermaas, E. H. & Toole, J. J. Selection of single-stranded DNA molecules that bind and inhibit human thrombin. *Nature* **355**, 564–566 (1992).
40. Tasset, D. M., Kubik, M. F. & Steiner, W. Oligonucleotide inhibitors of human thrombin that bind distinct epitopes. *J. Mol. Biol.* **272**, 688–698 (1997).
41. Grüner, S. et al. Anti-glycoprotein VI treatment severely compromises hemostasis in mice with reduced $\alpha_2\beta_1$ levels or concomitant aspirin therapy. *Circulation* **110**, 2946–2951 (2004).
42. Pleines, I. et al. Megakaryocyte-specific RhoA deficiency causes macrothrombocytopenia and defective platelet activation in hemostasis and thrombosis. *Blood* **119**, 1054–1063 (2012).
43. Deppermann, C. et al. Gray platelet syndrome and defective thrombo-inflammation in Nbeal2-deficient mice. *J. Clin. Invest.* **123**, 3331–3342 (2013).
44. Bakchoul, T. & Marini, I. Drug-associated thrombocytopenia. *Hematology Am. Soc. Hematol. Educ. Program* **2018**, 576–583 (2018).
45. Aster, R. H. & Bougie, D. W. Drug-induced immune thrombocytopenia. *N. Engl. J. Med.* **357**, 580–587 (2007).
46. Morowski, M. et al. Only severe thrombocytopenia results in bleeding and defective thrombus formation in mice. *Blood* **121**, 4938–4947 (2013).
47. Sekhon, U. D. S. et al. Platelet-mimicking procoagulant nanoparticles augment hemostasis in animal models of bleeding. *Sci. Transl. Med.* **14**, eabb8975 (2022).
48. Mast, A. E. & Ruf, W. Regulation of coagulation by tissue factor pathway inhibitor: implications for hemophilia therapy. *J. Thromb. Haemost.* **20**, 1290–1300 (2022).
49. Holtkotter, O. et al. Integrin α_2 -deficient mice develop normally, are fertile, but display partially defective platelet interaction with collagen. *J. Biol. Chem.* **277**, 10789–10794 (2002).
50. Jackson, B. et al. RhoA is dispensable for skin development, but crucial for contraction and directed migration of keratinocytes. *Mol. Biol. Cell* **22**, 593–605 (2011).
51. Knight, C. G. et al. Collagen-platelet interaction: Gly-Pro-Hyp is uniquely specific for platelet Gp VI and mediates platelet activation by collagen. *Cardiovasc. Res.* **41**, 450–457 (1999).
52. Schulte, V. et al. Targeting of the collagen-binding site on glycoprotein VI is not essential for in vivo depletion of the receptor. *Blood* **101**, 3948–3952 (2003).
53. Bergmeier, W. et al. Flow cytometric detection of activated mouse integrin $\alpha_{IIb}\beta_3$ with a novel monoclonal antibody. *Cytometry* **48**, 80–86 (2002).
54. Stegner, D. et al. Thrombopoiesis is spatially regulated by the bone marrow vasculature. *Nat. Commun.* **8**, 127 (2017).
55. Nieswandt, B., Bergmeier, W., Rackebrandt, K., Gessner, J. E. & Zirngibl, H. Identification of critical antigen-specific mechanisms in the development of immune thrombocytopenic purpura in mice. *Blood* **96**, 2520–2527 (2000).
56. Shida, Y. et al. Analysis of the role of von Willebrand factor, platelet glycoprotein VI-, and $\alpha_2\beta_1$ -mediated collagen binding in thrombus formation. *Blood* **124**, 1799–1807 (2014).

57. Nieswandt, B. et al. Expression and function of the mouse collagen receptor glycoprotein VI is strictly dependent on its association with the FcRγ chain. *J. Biol. Chem.* **275**, 23998–24002 (2000).
58. Gruner, S. et al. Multiple integrin–ligand interactions synergize in shear-resistant platelet adhesion at sites of arterial injury in vivo. *Blood* **102**, 4021–4027 (2003).
59. Nieswandt, B. et al. Glycoprotein VI but not α_vβ₃ integrin is essential for platelet interaction with collagen. *EMBO J.* **20**, 2120–2130 (2001).
60. Hofmann, S., Vögtle, T., Bender, M., Rose-John, S. & Nieswandt, B. The SLAM family member CD84 is regulated by ADAM10 and calpain in platelets. *J. Thromb. Haemost.* **10**, 2581–2592 (2012).
61. Bergmeier, W., Rackebrandt, K., Schroder, W., Zirngibl, H. & Nieswandt, B. Structural and functional characterization of the mouse von Willebrand factor receptor GPIb–IX with novel monoclonal antibodies. *Blood* **95**, 886–893 (2000).
62. Nieswandt, B. et al. Acute systemic reaction and lung alterations induced by an antiplatelet integrin GPIIb/IIIa antibody in mice. *Blood* **94**, 684–693 (1999).
63. Hemker, H. C. & Beguin, S. Thrombin generation in plasma: its assessment via the endogenous thrombin potential. *Thromb. Haemost.* **74**, 134–138 (1995).
64. Hemker, H. C. et al. Calibrated automated thrombin generation measurement in clotting plasma. *Pathophysiol. Haemost. Thromb.* **33**, 4–15 (2003).
65. Brouns, S. L. N. et al. Platelet-primed interactions of coagulation and anticoagulation pathways in flow-dependent thrombus formation. *Sci. Rep.* **10**, 11910 (2020).
66. van der Walt, S. et al. scikit-image: image processing in Python. *PeerJ* **2**, e453 (2014).
67. Schindelin, J. et al. Fiji: an open-source platform for biological-image analysis. *Nat. Methods* **9**, 676–682 (2012).
68. Göb, V. et al. Infarct growth precedes cerebral thrombosis following experimental stroke in mice. *Sci. Rep.* **11**, 22887 (2021).
69. Amich, J. et al. Three-dimensional light sheet fluorescence microscopy of lungs to dissect local host immune-*Aspergillus fumigatus* interactions. *mBio* **11**, e02752-19 (2020).
70. Kleinschnitz, C. et al. Targeting platelets in acute experimental stroke: impact of glycoprotein Ib, VI, and IIb/IIIa blockade on infarct size, functional outcome, and intracranial bleeding. *Circulation* **115**, 2323–2330 (2007).
71. Carstairs, K. C. The identification of platelets and platelet antigens in histological sections. *J. Pathol. Bacteriol.* **90**, 225–231 (1965).

Acknowledgements

We thank F. Lanza (Strasbourg, France) for providing *Gp5^{-/-}* mice, J. Pinnecker (Julius-Maximilians-Universität Würzburg, Würzburg, Germany) for assistance in LSFM image acquisition, S. Hartmann and J. Goldmann for excellent technical assistance (both from University Hospital Würzburg, Institute of Experimental Biomedicine, Würzburg, Germany) and M. Spindler for excellent graphical assistance (University Hospital Würzburg, Institute of Experimental Biomedicine, Würzburg, Germany). Funding was provided by the German Research Foundation (Ni556/14-1, B.N.; SFB 1525, project number 453989101; TR240, project number 374031971; INST 93/1022-1), the National Institutes of Health (HL082808, R.L.; UM1 HL120877, W.R.), the European Union (Thrombo-Inflame, EFRE–Europäischer Fonds für

regionale Entwicklung, Bavaria) and the Rudolf Virchow Centre for Integrative and Translational Bioimaging.

Author contributions

Conceptualization: S.B., J.W.M.H., W.R., D.S. and B.N. Methodology: Y.W., R.L., K.H., K.G.H., W.R. and B.N. Investigation: S.B., P.Ö., M.N., A.Z., Z.M.R., J.W.M.H., M.K.S., G.S., D.S. and B.N. Visualization: S.B. Funding acquisition: B.N. and R.L. Supervision: D.S. and B.N. Writing (original draft): S.B., W.R. and B.N. Writing (review and editing): S.B., P.Ö., R.L., K.H., M.K.S., K.G.H., Z.M.R., J.W.M.H., W.R., D.S. and B.N.

Competing interests

S.B., D.S. and B.N. hold a patent on recombinant GPV for treating thrombotic diseases reporting sGPV (lacking a functional transmembrane domain) for use in the treatment or prevention of thrombotic diseases. Data on rhGPV preventing thrombus formation in vivo and reducing infarct volume in a tMCAO model in this study are partly covered by the patent (patent applicant, Julius-Maximilians-Universität Würzburg; inventors, B.N., D.S., S.B.; patent published, title, soluble glycoprotein V for treating thrombotic diseases; WO 2017/109212; US patent no. US 11,028,144 B2).

Additional information

Extended data is available for this paper at <https://doi.org/10.1038/s44161-023-00254-6>.

Supplementary information The online version contains supplementary material available at <https://doi.org/10.1038/s44161-023-00254-6>.

Correspondence and requests for materials should be addressed to David Stegner or Bernhard Nieswandt.

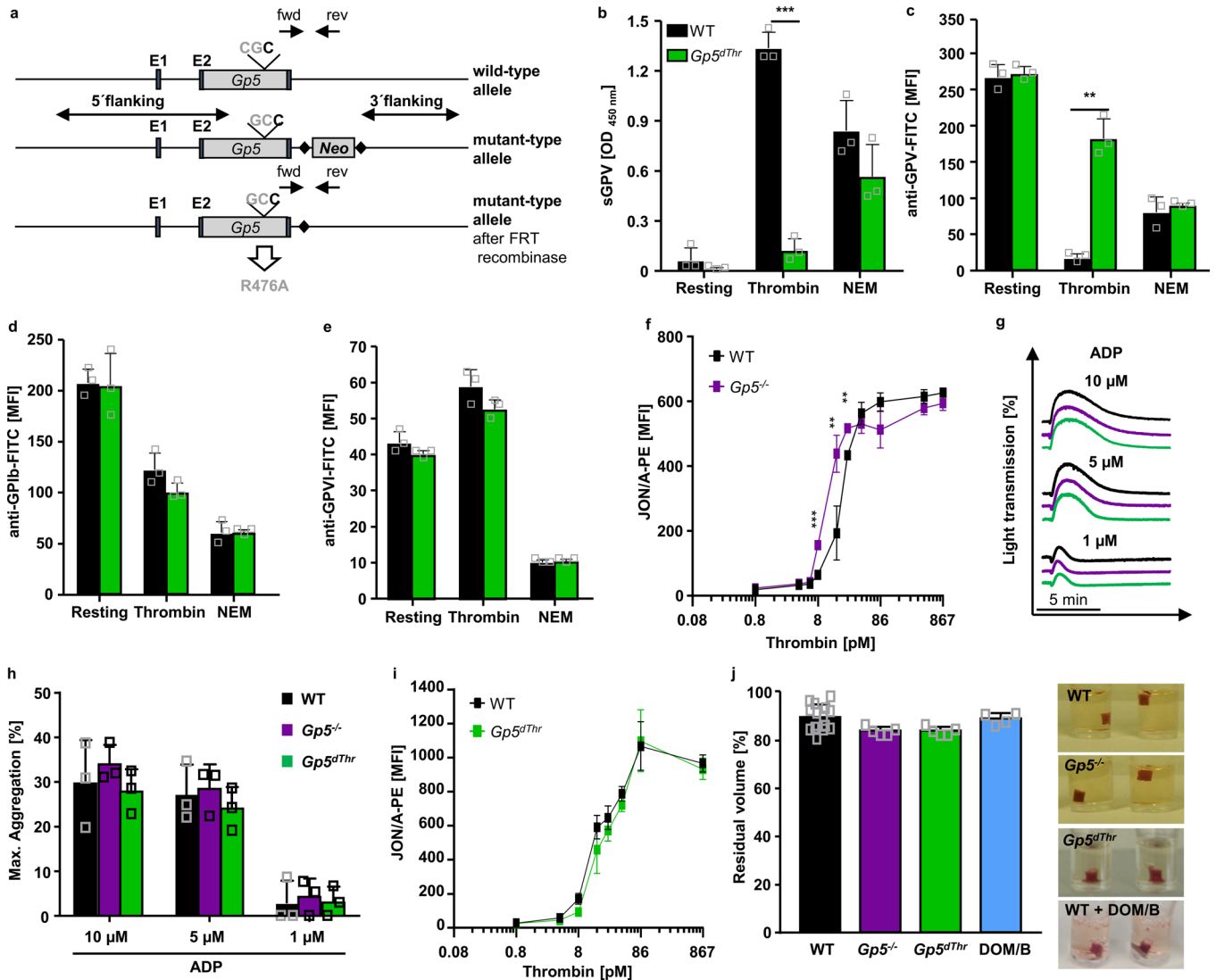
Peer review information *Nature Cardiovascular Research* thanks Cedric Duval, Louise D. McCullough and the other, anonymous, reviewer(s) for their contribution to the peer review of this work.

Reprints and permissions information is available at www.nature.com/reprints.

Publisher's note Springer Nature remains neutral with regard to jurisdictional claims in published maps and institutional affiliations.

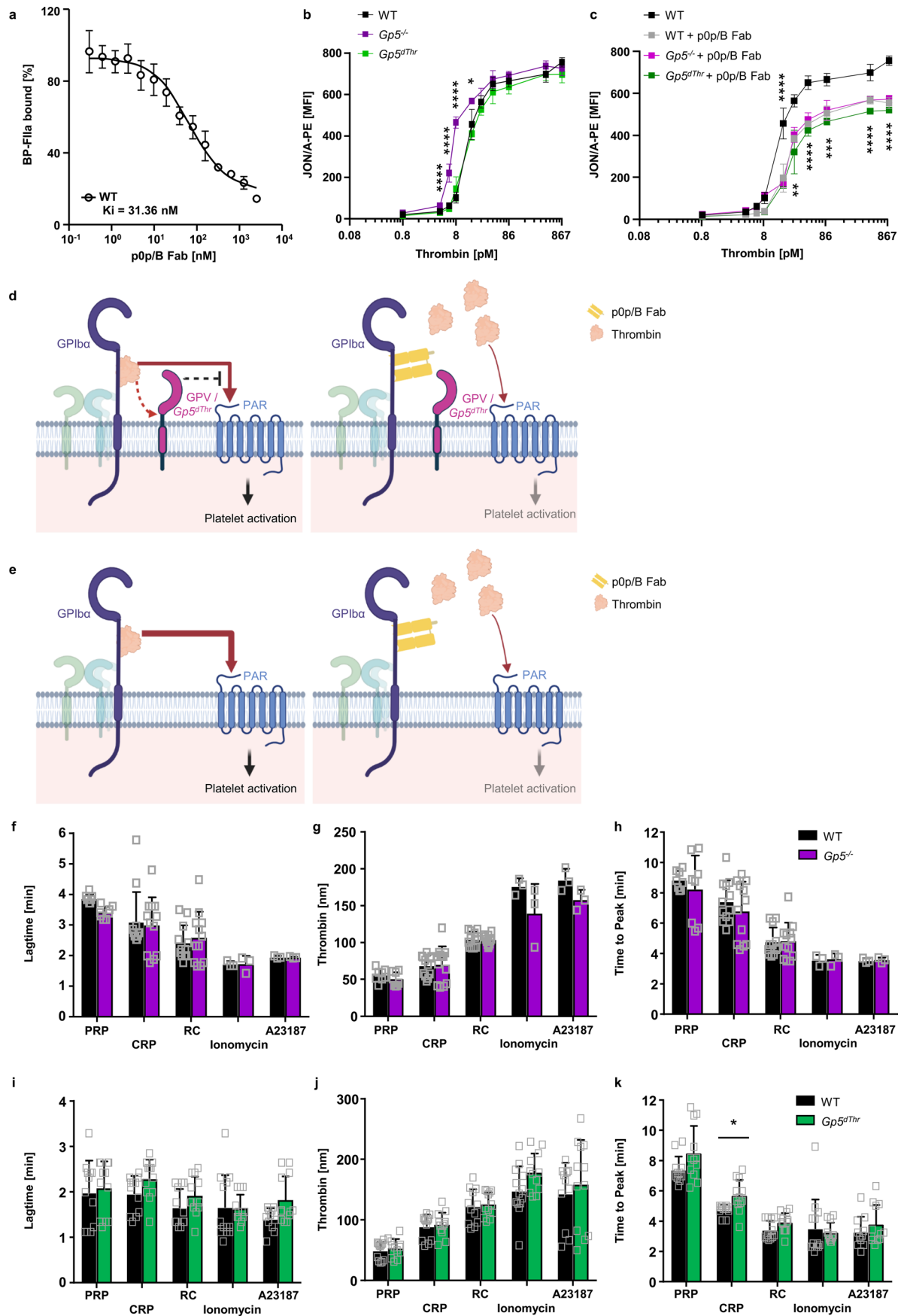
Open Access This article is licensed under a Creative Commons Attribution 4.0 International License, which permits use, sharing, adaptation, distribution and reproduction in any medium or format, as long as you give appropriate credit to the original author(s) and the source, provide a link to the Creative Commons license, and indicate if changes were made. The images or other third party material in this article are included in the article's Creative Commons license, unless indicated otherwise in a credit line to the material. If material is not included in the article's Creative Commons license and your intended use is not permitted by statutory regulation or exceeds the permitted use, you will need to obtain permission directly from the copyright holder. To view a copy of this license, visit <http://creativecommons.org/licenses/by/4.0/>.

© The Author(s) 2023



Extended Data Fig. 1 | R476A point mutation renders GPV insensitive for thrombin-induced cleavage in *Gp5^{dThr}* mice but does not alter platelet reactivity towards thrombin. (a) Simplified targeting strategy. *Gp5^{dThr}* mice were generated by introduction of the point mutation R476A in the thrombin cleavage site. (b-e) Washed platelets were left untreated or stimulated with 867 pM thrombin (in the presence of 40 µg/ml integrilin and 5 µM EGTA to prevent platelet aggregation) or 2 mM *N-ethylmaleimide* (NEM) to induce metalloproteinase-induced shedding of GPV. (b) After stimulation, sGPV levels in the platelet supernatant were measured using a mGPV ELISA. Mean ± SD. n = 3 mice per group, 3 independent experiments, two-tailed unpaired t-test with Welch's correction, p = 0.0001. (c-e) Stimulated platelets were incubated with saturating amounts of fluorophore-conjugated antibodies for 15 min at RT and the surface expression of GPV (c), GPIb (d) and GPVI (e) was immediately analysed by flow cytometry. Mean ± SD. n = 3 mice per group, 3 independent experiments, (c) two-tailed unpaired t-test with Welch's correction, p = 0.0067.

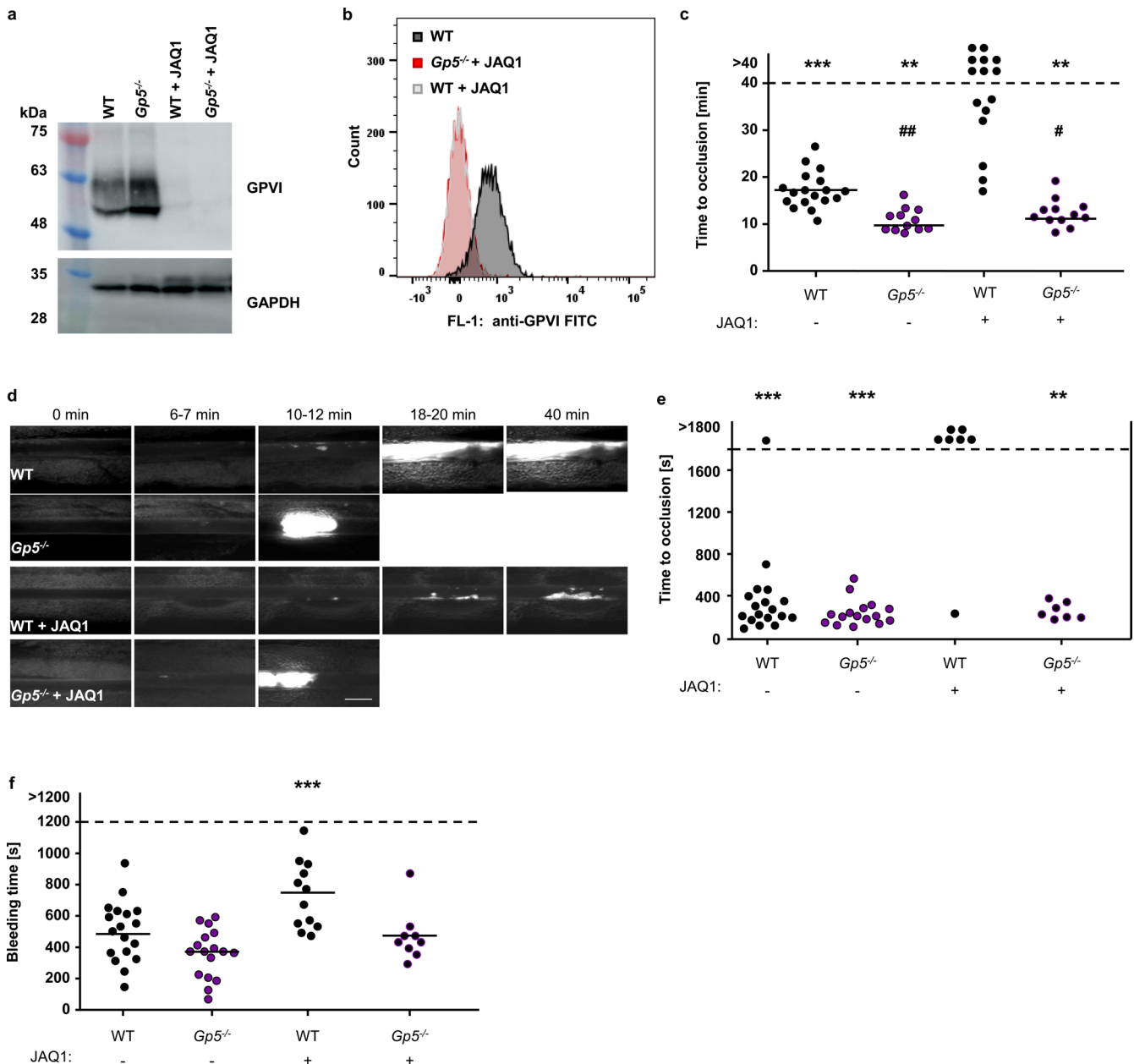
(f) Increased αIIbβ3 integrin activation measured by JON/A-PE staining of GPV-deficient platelets at threshold thrombin concentrations. Mean ± SD, n = 4 mice, 5 independent experiments, two-tailed unpaired t-test with Welch's correction. 8.6 pM thrombin: p = 0.0009, 17.35 pM thrombin: p = 0.0039, 26 pM thrombin: p = 0.0026 (g, h) Platelet-rich plasma (PRP) was stimulated with ADP and light transmission of PRP was recorded on a Apact four-channel aggregometer over 10 min. Representative curves (g) and maximum aggregation (h) for n = 3 mice of 3 independent experiments expressed as mean ± SD. (i) Flow cytometry reveals unaltered reactivity of *Gp5^{dThr}* platelets upon thrombin stimulation compared to WT controls. Mean ± SD, n = 4 mice, 5 independent experiments. (j) Clot formation in PRP was induced by the addition of thrombin and CaCl₂ and clot retraction was monitored over time. Residual volume of serum after clot retraction was measured. Mean ± SD. WT: n = 14, *Gp5^{-/-}*: n = 5, *Gp5^{dThr}*: n = 5, WT + DOM/B: n = 4 mice, 2 independent experiments. Representative images at 90 min after initiation of clot retraction. *p < 0.05; **p < 0.01; ***p < 0.001.



Extended Data Fig. 2 | See next page for caption.

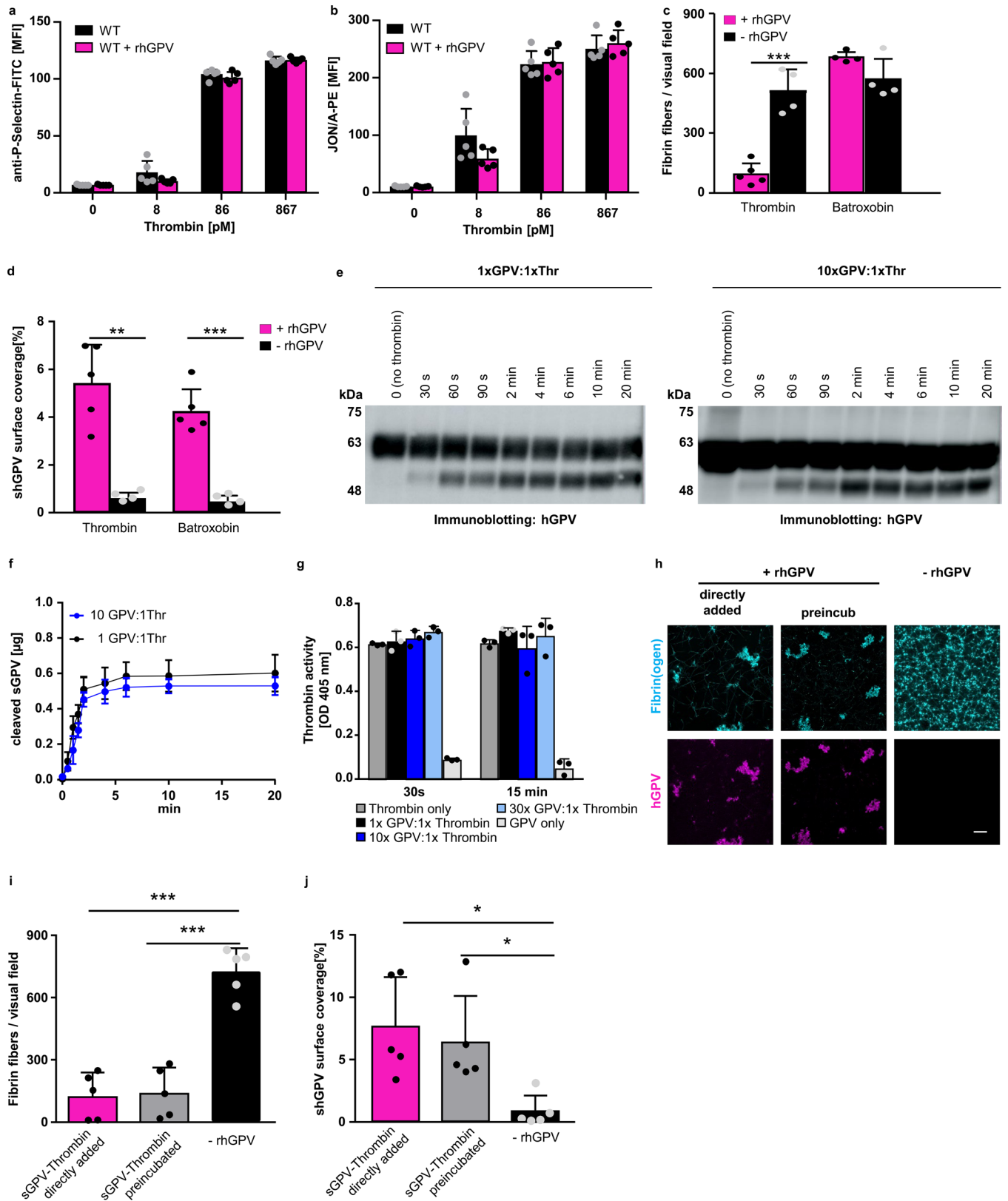
Extended Data Fig. 2 | GPV regulates platelet responsiveness to thrombin by interference with GPIIb α -dependent PAR signaling. (a) Platelets were incubated with increasing concentrations of pOp/B Fab fragments and BP-FIIa binding was assessed by flow cytometry. $n = 4$ mice, 2 independent experiments. (b, c) The thrombin-binding site on GPIIb α was blocked by pOp/B Fab and α IIb β 3 integrin activation (JON/A-PE binding) of GPV-mutant and WT platelets measured by flow cytometry upon thrombin stimulation. (b, c) were measured in one experiment. Mean \pm SD. $n = 4$ mice per group, 4 independent experiments. One-way ANOVA followed by Tukey's multiple comparisons test. (d) Scheme of GPIIb-thrombin and GPV-thrombin interactions. GPIX (green), GPIIb β (light blue), GPIIb α and GPV (magenta) form a complex on the platelet surface. Thrombin binds to GPIIb α via a high affinity binding site, cleaves GPV and activates platelets via PARs. The anti-GPIIb α Fab pOp/B blocks the thrombin binding site on GPIIb α and thereby reduces thrombin-mediated platelet activation. Both, GPV and

Gp5^{dThr} act as an inhibitor of GPIIb-mediated PAR activation. In the absence of GPV (e), access of thrombin to PARs is facilitated leading to increased platelet activation. (d, e) created with BioRender. (f-k) TF-initiated thrombin generation was measured in platelet-rich plasma (PRP) upon platelet activation. Platelets were left unstimulated (PRP) or activated by incubation with collagen-related peptide (CRP) (20 μ g/ml), rhodocytin (RC, 1 μ g/ml), ionomycin (10 μ M) or A23187 (10 μ M) for 10 min at 37 $^{\circ}$ C. Thrombin generation was triggered with tissue factor/ CaCl_2 . Lag time (f, i), maximal thrombin concentration (g, j) and time to peak (h, k) were determined. Values are depicted as mean \pm SD. (f-h) $n = 12$ (CRP, RC), $n = 8$ (PRP), $n = 3$ (A23187, ionomycin). (i-k) $n = 12$ (Gp5^{dThr}: all conditions, WT: PRP, CRP, RC); WT: $n = 13$ (ionomycin), WT: $n = 11$ (A23187) mice, at least 2 independent experiments. Two-tailed unpaired t-test with Welch's correction, $p = 0.0106$. * $p < 0.05$; ** $p < 0.01$; *** $p < 0.001$; **** $p < 0.0001$.



Extended Data Fig. 3 | Absence of GPVI restores thrombotic and haemostatic defects in the absence of GPVI. GPVI was depleted from the platelet surface by injection of the anti-GPVI mAb JAQ1. Confirmation of GPVI depletion by Western blot analysis (a) and flow cytometry (b); representative of 3 independent experiments. (c) Quantification and representative images (scale bar: 50 μ m) (d) of thrombus formation upon $FeCl_3$ -induced injury of mesenteric arterioles. Thrombus formation in no more than two arterioles of each mouse were analysed; data points represent measurements of one arteriole. WT: 18 arterioles of 11 mice, *Gp5^{-/-}*: 12 arterioles of 8 mice, WT + JAQ1: 15 arterioles of 8 mice, *Gp5^{-/-}* + JAQ1: 12 arterioles of 7 mice. Two-tailed Fisher's exact test for open vs. occluded vessels, $p = 0.0005$ (WT vs. WT + JAQ1), $p = 0.0031$ (*Gp5^{-/-}* vs. WT + JAQ1; *Gp5^{-/-}* + JAQ1 vs. WT + JAQ1); one-way ANOVA followed by Tukey's test for multiple comparisons to compare occluded vessels, ### $p = 0.0034$ (WT vs. *Gp5^{-/-}*), # $p = 0.0401$ (WT vs. *Gp5^{-/-}* + JAQ1) compared to JAQ1-treated

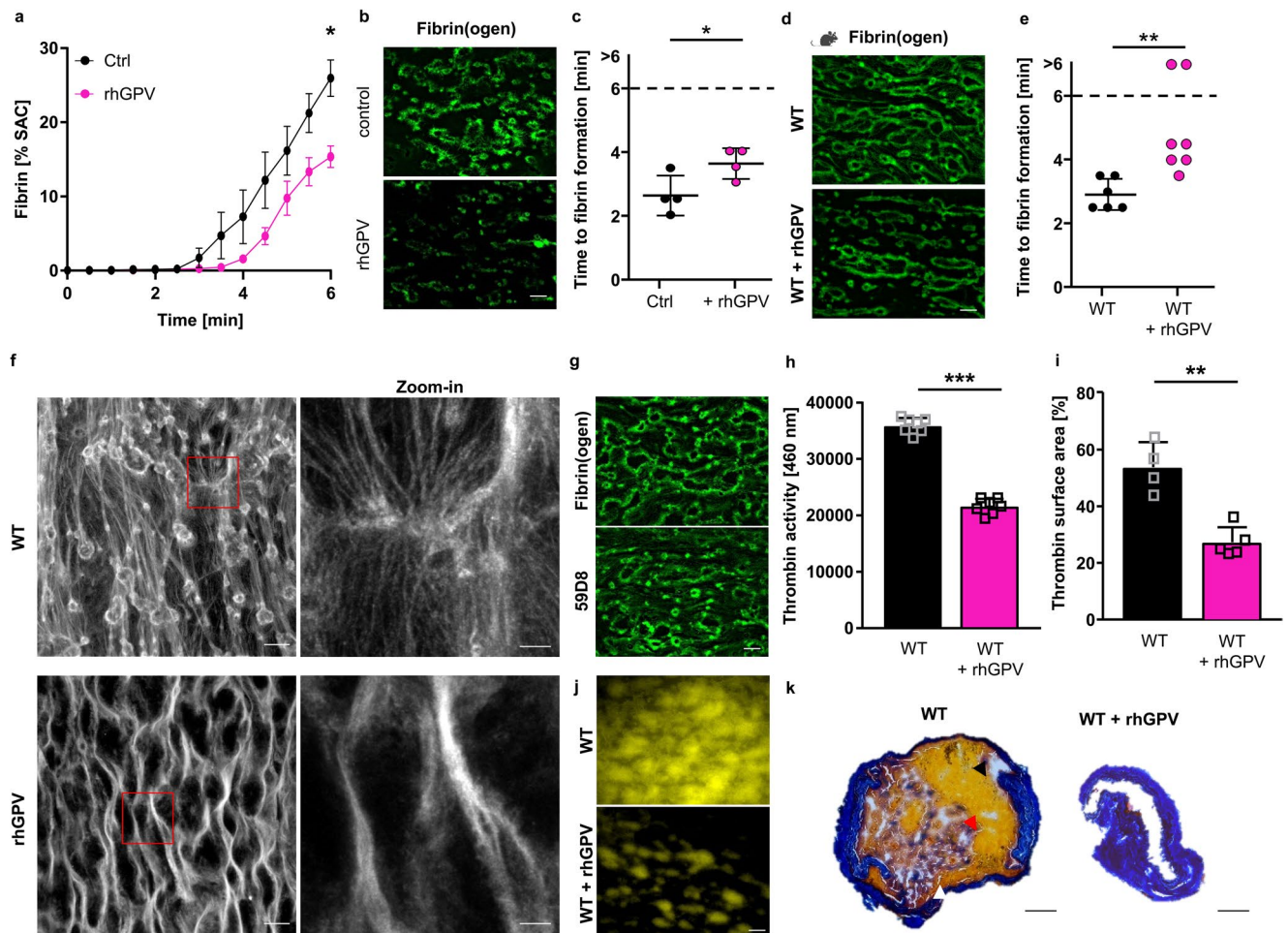
WT mice ($p = 0.0031$). * compared to JAQ1-treated WT mice. (e) The abdominal aorta was mechanically injured by a single firm compression with a forceps and blood flow was monitored with a Doppler flowmeter. Time to cessation of blood flow is shown. Each symbol represents one mouse. Two-tailed Fisher's exact test for open vs. occluded vessels, one-way ANOVA followed by Dunn's test for multiple comparisons to compare occluded vessels. WT: $n = 18$, *Gp5^{-/-}*: $n = 16$, WT + JAQ1: $n = 7$, *Gp5^{-/-}* + JAQ1: $n = 7$, ***WT + JAQ1 vs. WT and vs. *Gp5^{-/-}*: $p < 0.0001$, **WT + JAQ1 vs. *Gp5^{-/-}* + JAQ1: $p = 0.0047$), ### compared to untreated WT mice (WT + JAQ1: $p = 0.0003$). (f) Hemostatic function was assessed using a tail bleeding assay on filter paper. Each symbol represents one mouse. WT: $n = 18$, *Gp5^{-/-}*: $n = 17$, WT + JAQ1: $n = 12$, *Gp5^{-/-}* + JAQ1: $n = 9$, one-way ANOVA followed by Dunn's test for multiple comparisons to compare occluded vessels, $p = 0.0001$ *, # $p < 0.05$; **, ## $p < 0.01$; ***, ### $p < 0.001$.



Extended Data Fig. 4 | See next page for caption.

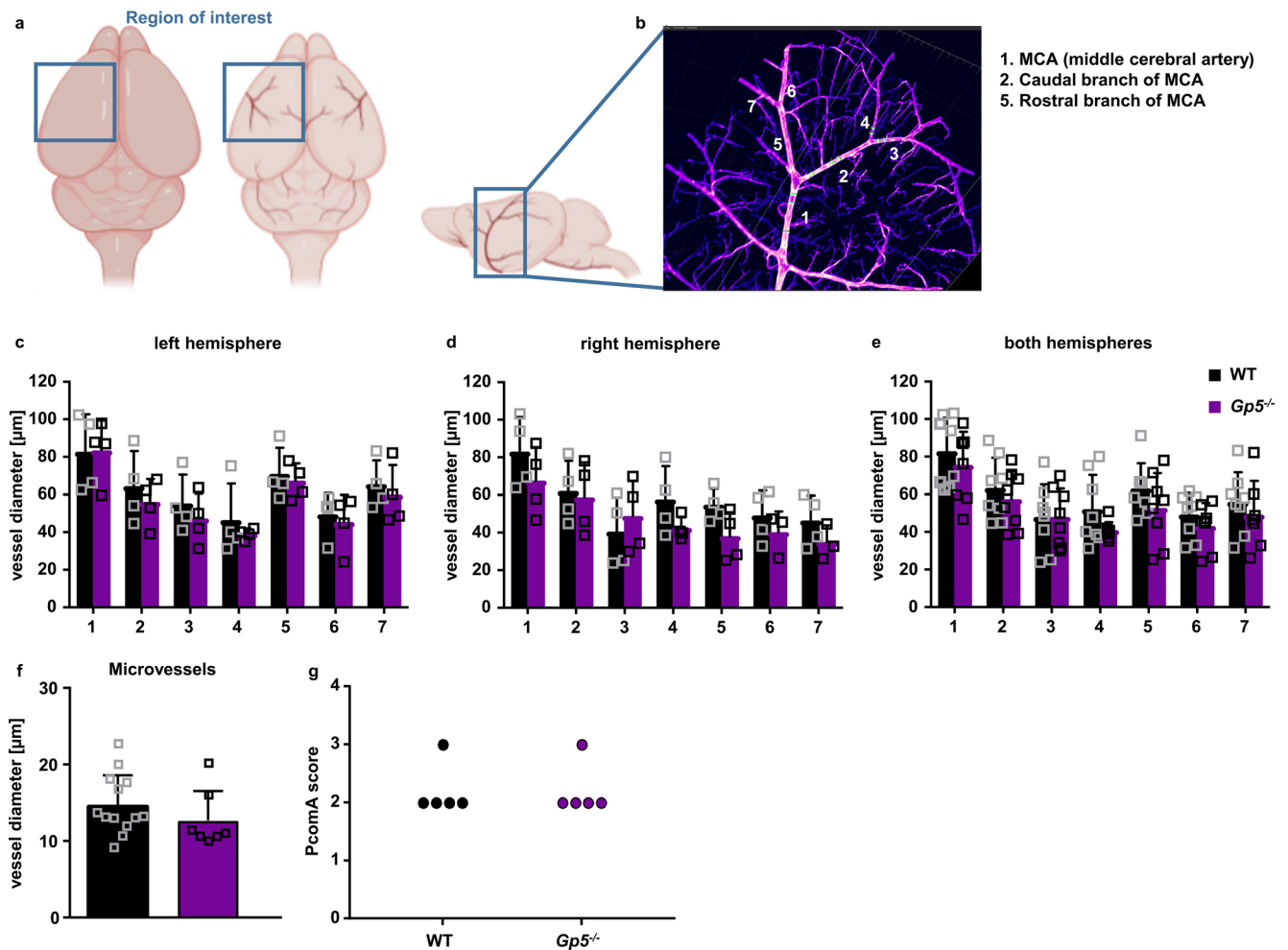
Extended Data Fig. 4 | shGPV directly interacts with thrombin. **(a)** P-selectin exposure at threshold thrombin concentrations in rhGPV-treated (20 µg/ml) and WT platelets. Mean ± SD of n = 5 mice, 3 independent experiments. **(b)** Unaltered αIIbβ3 integrin activation (JON/A-PE binding) at threshold thrombin concentrations in the presence of rhGPV. Mean ± SD, n = 5 mice, 3 independent experiments. Welch's test. Fibrin fibres **(c)** and hGPV staining **(d)** were quantified upon static fibrin polymerization induced by thrombin or batroxobin in the absence or presence of rhGPV. Mean ± SD, **(c)** -rhGPV: n = 4, rhGPV: n = 5 (Thrombin), n = 4 (Batroxobin), two-tailed unpaired t-test with Welch's correction, p = 0.0020, **(d)** -rhGPV: n = 4, rhGPV: n = 5 independent samples (mean of 2 ROI per sample), two-tailed unpaired t-test with Welch's correction, p = 0.0029 (thrombin), p = 0.0006 (batroxobin). **(e-g)** rhGPV and thrombin were incubated at equimolar ratio (1:1) or with an excess of rhGPV (10:1 ratio) and thrombin-mediated cleavage of rhGPV was assessed over time by immunoblotting. **(f)** Quantification of thrombin-cleaved sGPV over time.

Mean ± SD, n = 5 independent western blot experiments. **(g)** rhGPV and thrombin were incubated at equimolar ratio (1:1) or with an excess of rhGPV (10:1, 30:1 ratio) and the activity of thrombin was determined using a chromogenic thrombin substrate. Mean ± SD, n = 3 independent samples, representative of 4 experiments. **(h)** Maximum projection of static fibrin polymerization induced by thrombin in the absence or presence of rhGPV (30:1 ratio). Thrombin and rhGPV were either directly added or preincubated for 10 min prior induction of polymerization. Fluorophore labelled fibrin(ogen): cyan, staining for hGPV: magenta. Scale bar: 20 µm. Quantification of fibrin fibres **(i)** and hGPV staining **(j)**. Mean ± SD, n = 5 biologic samples (mean of 2 ROI per sample), **(i)** one-way ANOVA followed by Tukey's multiple comparison test, p > 0.0001, **(j)** Kruskal-Wallis test followed by Dunn's multiple comparisons test, p = 0.0175 (directly vs. no rhGPV), p = 0.0327 (preincubated vs. no rhGPV). *, p < 0.05; **p < 0.01; ***p < 0.001.



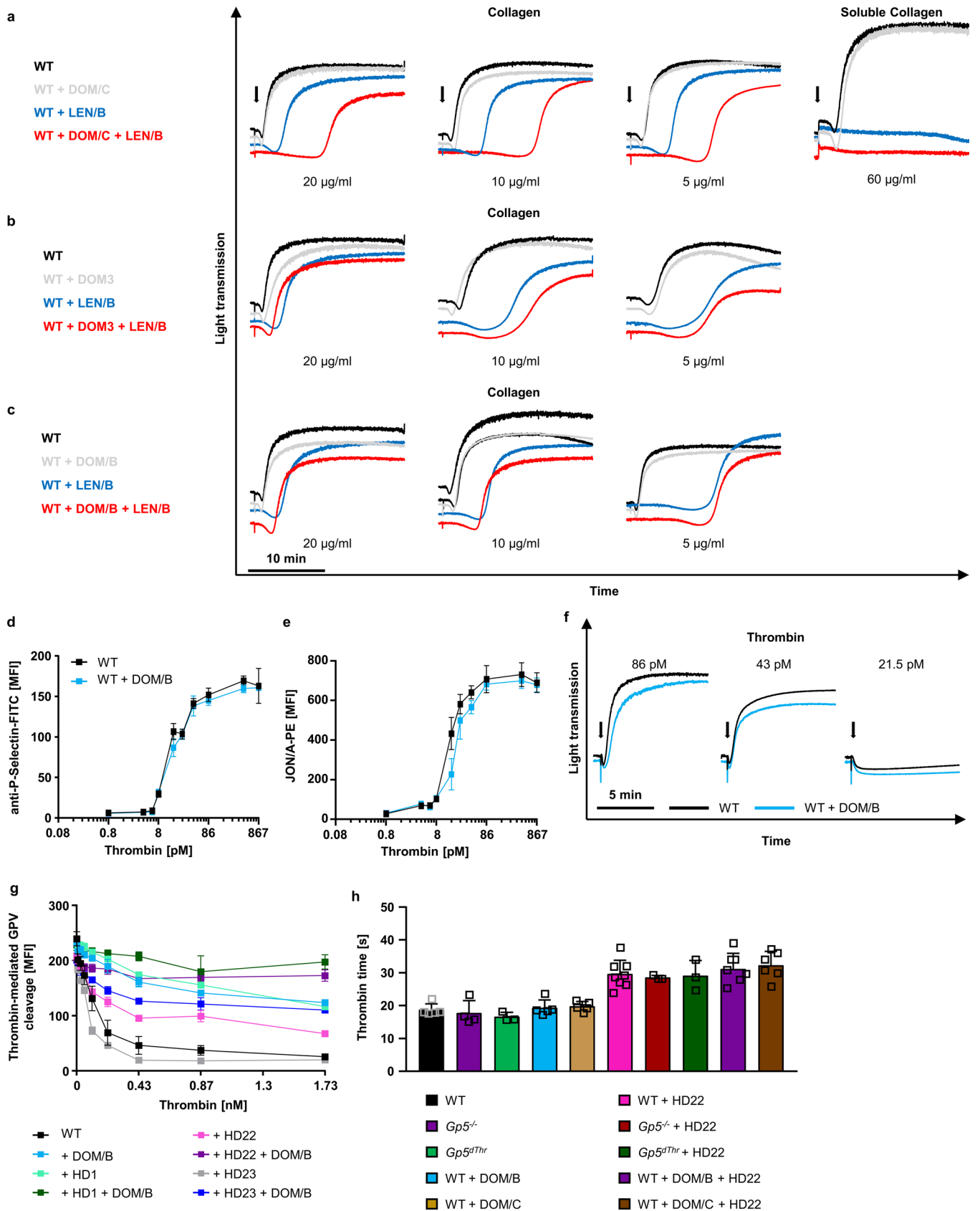
Extended Data Fig. 5 | rhGPV delays and reduces fibrin formation. Recalcified whole blood was incubated *in vitro* with 20 $\mu\text{g}/\text{ml}$ rhGPV prior to perfusion over collagen/TF spots. Quantification of fibrin generation during blood flow in human (a–c) and mouse blood (d, e). (a) Mean \pm SEM; $n = 4$ donors, 3 independent experiments, two-tailed paired t-test, $p = 0.0133$. Ctrl: human donor. (b, d) Representative images displaying decreased fibrin formation after rhGPV-treatment. Scale bar: 20 μm . (c) Time to fibrin formation in rhGPV-treated human blood. Ctrl: Human control. Mean \pm SD, $n = 4$ donors, 3 independent experiments, two-tailed paired t-test, $p = 0.0163$. (e) Time to fibrin formation in rhGPV-treated WT blood. Mean \pm SD, WT: $n = 6$, WT + rhGPV: $n = 7$, 3 independent experiments, two-tailed Mann-Whitney test, $p = 0.0023$. (f) Analysis of fibrin fibrils by laser scanning confocal microscopy. Fibrin fibres were visualised using a Leica SP8 confocal microscope, 63x oil, Hyvolution mode, z-step size: 0.1 μm , 15 μm z-size. Images were deconvolved using Huygens Software. Maximum projection. Scale bar: 20 μm . Zoom-in: 5 μm .

Representative of $n = 5$ mice. (g) Fibrin formation using Fibrin(ogen)A488 or the anti-Fibrin antibody 59D8. Representative images, scale bar: 20 μm . (h) Thrombin activity was determined in the outflow of the flow chamber using a fluorogenic thrombin substrate and measured immediately after sample collection. Mean \pm SD; $n = 7$ mice, 3 independent experiments, two-tailed unpaired t-test with Welch's correction, $p < 0.0001$. (i) Thrombin activity in flow chambers was determined using the fluorogenic thrombin substrate Z-GGR-AMC. (j) Representative images of (i). Mean \pm SD; WT: $n = 4$, WT + rhGPV: $n = 5$ mice, 2 independent experiments, two-tailed unpaired t-test with Welch's correction, $p = 0.0039$. Scale bar: 20 μm . (k) Carstairs staining of the abdominal aorta after mechanical injury-induced thrombus formation in a WT and rhGPV-treated mouse (red blood cells: yellow (indicated with black arrowhead), fibrin: bright red (red arrowhead), platelets: navy blue (white arrowhead), collagen: blue). Scale bar: 100 μm . rhGPV: 20 $\mu\text{g}/\text{ml}$. SAC: surface area coverage. * $p < 0.05$; ** $p < 0.01$; *** $p < 0.001$.



Extended Data Fig. 6 | Unaltered MCA vessel diameter in $Gp5^{-/-}$ mice. Optically transparent brain samples of $Gp5^{-/-}$ and WT mice were imaged using light sheet fluorescence microscopy (LSFM). **(a)** Due to its conserved branching and its easy recognition, we focused on the region around the middle cerebral artery (MCA) to allow better comparability between the samples. **(b)** We analysed the vessel diameter of the MCA (1) and 2 subsequent branches of the caudal (2) and rostral (5) branch of the MCA using Imaris Software. **(c-e)** Vessels in the left, right hemisphere and the combination of both hemispheres did not show any

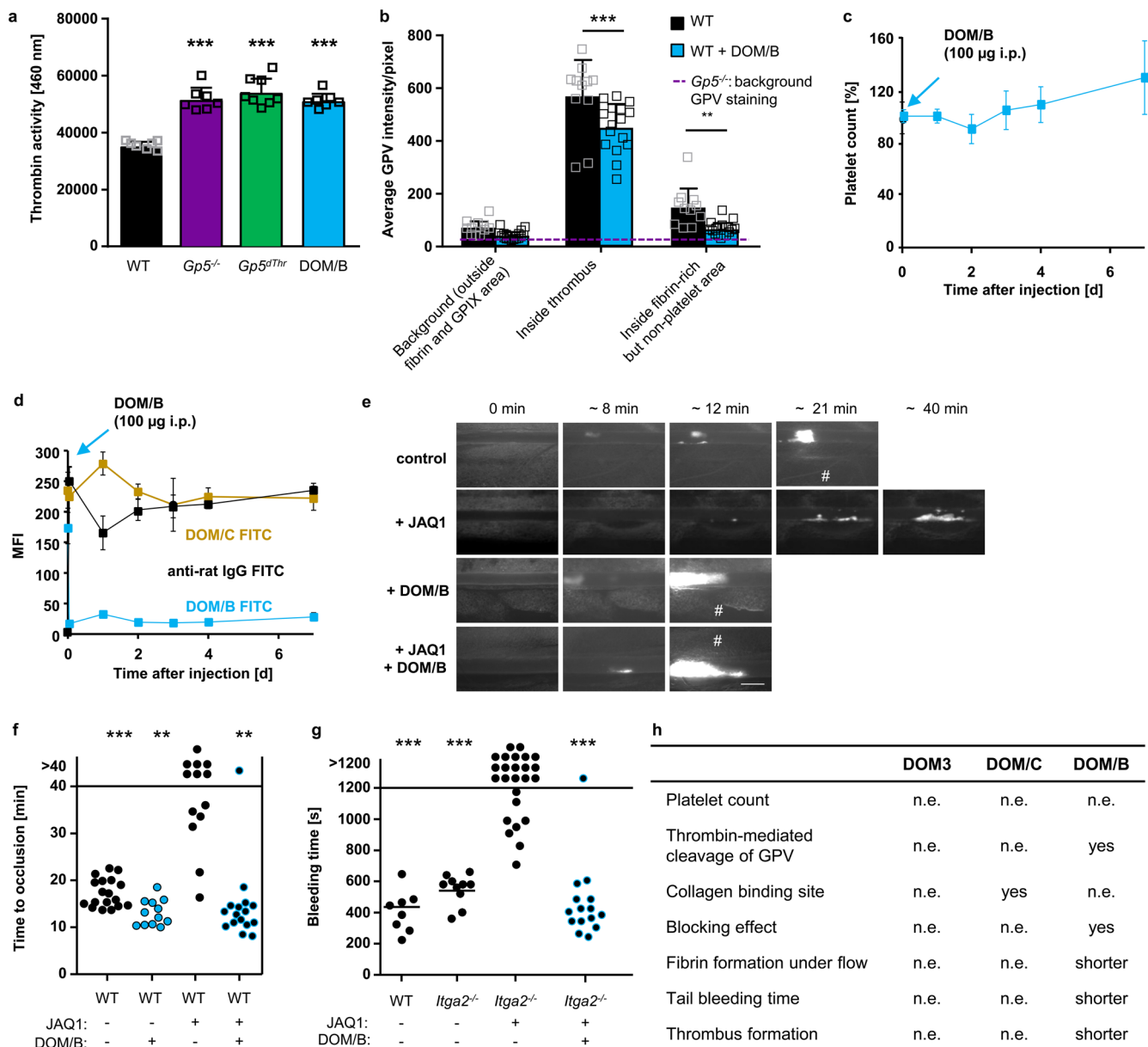
difference between GPV-deficient and WT mice. Mean \pm SD. $n = 4$ mice. **(f)** Vessel diameters of microvessels in the brain were comparable between $Gp5^{-/-}$ and WT mice. Mean \pm SD. WT: $n = 13$ vessels of 4 mice, $Gp5^{-/-}$: $n = 7$ vessels of 4 mice. Two-tailed unpaired t-test with Welch's correction. **(g)** PcomA scores (posterior communicating artery) were determined in brains from mice that were perfused with PBS followed 3 ml black ink diluted in 4% PFA (1:5 v/v) and comparable between $Gp5^{-/-}$ and WT mice. $n = 5$. Mann-Whitney test. (a, b) created with BioRender.



Extended Data Fig. 7 | See next page for caption.

Extended Data Fig. 7 | DOM/B does not alter platelet responses upon stimulation with collagen or thrombin *in vitro*, despite interfering with thrombin-mediated cleavage of GPV. (a-c) Washed platelets were incubated *in vitro* with 10 µg/ml of the indicated antibodies for 5 min and stimulated with Horm or soluble collagen. Light transmission was recorded on an Apact four-channel aggregometer over 20 min. Representative aggregation curves of n = 3, 2 independent experiments. LEN/B: anti-α2 integrin antibody⁵¹. **(d, e)** Flow cytometry reveals unaltered reactivity of DOM/B-treated WT platelets upon thrombin stimulation compared to WT controls. Mean ± SD. n = 3 mice, 4 independent experiments, two-tailed unpaired t-test with Welch's correction. **(f)** Aggregation upon thrombin-stimulation is not affected in the presence of DOM/B. Light transmission was recorded on an Apact four-channel

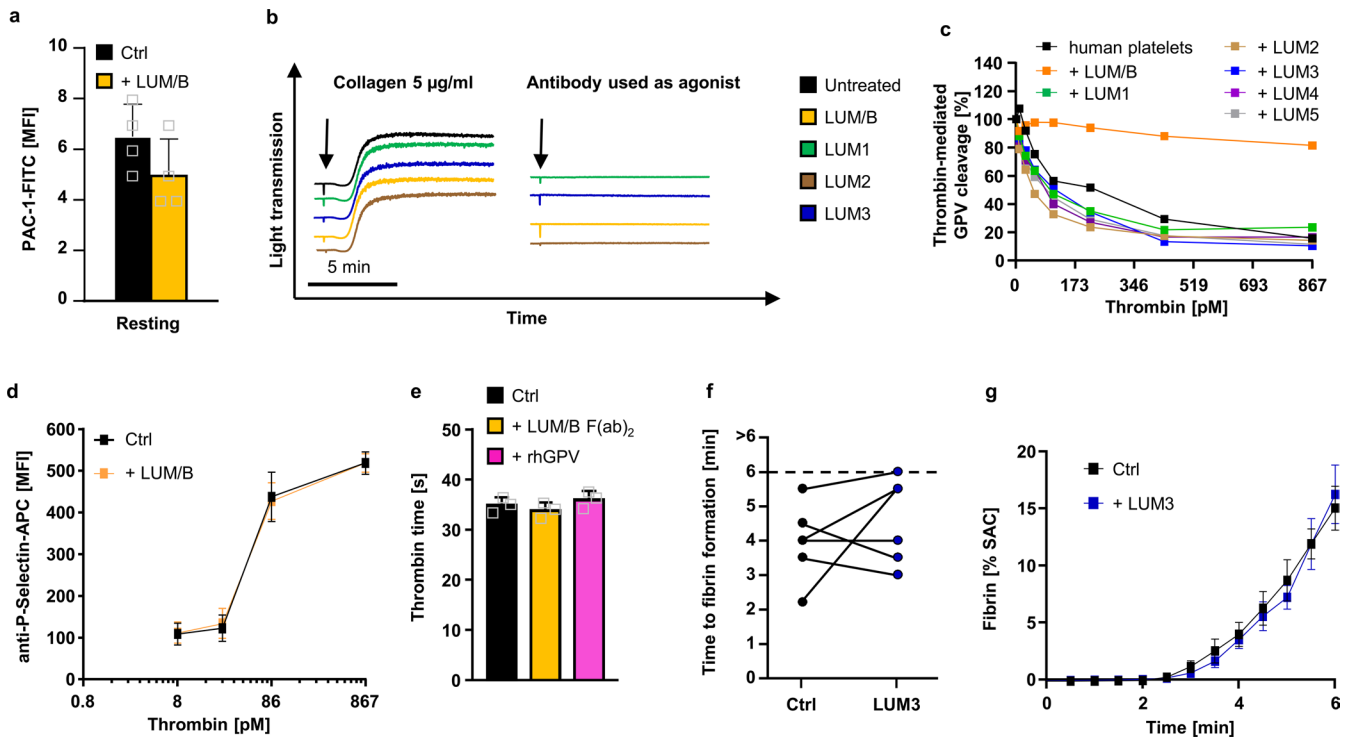
aggregometer over 10 min. Representative curves of n = 3, 3 individual experiments. **(g)** Thrombin exosites I and II were blocked by the aptamers HD1 and HD22, respectively. Platelets were incubated with the indicated antibody (10 µg/ml) prior to thrombin stimulation. Thrombin-mediated cleavage of GPV was assessed by flow cytometry. Mean ± SD. n = 3 mice, 3 independent experiments. **(h)** Thrombin clotting time was assessed using a ball coagulometer in GPV mutant or anti-mGPV mAb treated PRP in the presence or absence of HD22. Antibody concentration: 10 µg/ml; aptamer concentration: 1.5 µM f.c., thrombin: 17 nM. Mean ± SD. WT, WT + DOM/B, WT + DOM/C: n = 5, *Gp5^{-/-}*: n = 4, *Gp5^{ΔThr}*, *Gp5^{-/-}*+HD22, *Gp5^{ΔThr}* + HD22: n = 3, WT + DOM/B + HD22, WT + DOM/C + HD22: n = 6, WT + HD22: n = 8. One-way ANOVA followed by Dunn's test for multiple comparisons.



Extended Data Fig. 8 | DOM/B restores hemostasis and thrombus formation in the absence of GPVI, thereby reproducing the *Gp5^{-/-}* phenotype. (a)

Recalcified blood was perfused over collagen/TF spots. Thrombin activity was determined in the outflow using a fluorogenic thrombin substrate and measured immediately. Mean ± SD. WT, *Gp5^{-/-}*, WT + DOM/B: n = 7, *Gp5^{dThr}*: n = 8, one-way ANOVA followed by Tukey's multiple comparisons test, $p < 0.0001$ for all groups compared to WT. (b) Recalcified blood was perfused over collagen/TF spots. Samples were stained for platelets (anti-GPIX), fibrin(ogen) and GPV, fixed and analysed with a Zeiss Airyscan microscope. Quantification of GPV intensities inside fibrin-rich, non-platelet area. Background GPV intensity in *Gp5^{-/-}* images is displayed as dashed line (n = 4). Mean ± SD. Two-way ANOVA followed by Tukey's multiple comparisons test, $p < 0.0001$ (inside thrombus), $p = 0.0089$ (inside fibrin), WT, n = 11, WT + DOM/B: n = 16. (c, d) WT mice were injected with DOM/B (100 µg i.p.) and platelet count was assessed for 7 days (c). Platelet count at d0 was set to 100%. Mean ± SD, n = 5 mice, 2 independent experiments. (d) GPV platelet surface expression was assessed by flow cytometry for up to 7 days after DOM/B injection. Mean ± SD, n = 5 mice, 2 independent experiments. Receptor opsonization was measured using an anti-rat IgG FITC antibody. (e-g)

GPVI was depleted from the platelet surface by injection of the anti-GPVI mAb JAQ1. Representative images (e) and quantification (f) of thrombus formation upon FeCl_3 -induced injury of mesenteric arterioles in WT mice after JAQ1 and DOM/B treatment. Thrombus formation in no more than two arterioles of each mouse was analysed; data points represent measurements of one arteriole. WT: n = 18 arterioles of 10 mice, WT + DOM/B: n = 12 arterioles of 6 mice, WT + JAQ1: n = 13 arterioles of 7 mice, WT + DOM/B + JAQ1: n = 16 arterioles of 8 mice, two-tailed Fisher's exact test to compare occluded vs. non-occluded vessels was used. $p = 0.0007$ (vs. WT), $p = 0.0052$ (vs. WT + DOM/B), $p = 0.0011$ (vs. WT + JAQ1 + DOM/B), # indicates vessel occlusion. Scale bar: 50 µm. (g) Mice lacking both collagen receptors GPVI and $\alpha 2$ were treated with DOM/B and hemostatic function was assessed using a tail bleeding assay on filter paper. Each symbol represents one mouse. WT: n = 8, *Itga2^{-/-}*: n = 10, *Itga2^{-/-}* + JAQ1: n = 25, *Itga2^{-/-}* + JAQ1 + DOM/B: n = 16, two-tailed Fisher's exact test for open vs. occluded vessels. $p = 0.0009$ (vs. WT), $p = 0.0003$ (vs. *Itga2^{-/-}*), $p = 0.0001$ (vs. *Itga2^{-/-}* + JAQ1 + DOM/B). (h) Summary of the effects of the different anti-mGPV antibodies. n.e.: no effect. * $p < 0.05$; ** $p < 0.01$; *** $p < 0.001$.



Extended Data Fig. 9 | LUM/B has no effect on thrombin-mediated platelet activation. (a) Human platelets were incubated with 10 µg/ml LUM/B prior to flow cytometric analysis of PAC1-binding. Mean ± SD, n = 4 donors. (b) Human platelets were incubated with the indicated anti-hGPV mAbs light transmission was recorded on a Aparent four-channel aggregometer over 10 min. Representative curves for n = 3. (c) Human platelets were incubated with the indicated antibody (10 µg/ml) prior to thrombin stimulation. Thrombin-mediated cleavage of GPV was assessed by flow cytometry. Mean ± SD, n = 2 donors, 3 independent experiments. (d) Flow cytometry reveals unaltered reactivity of LUM/B-treated platelets upon thrombin stimulation compared

to controls. (e) Neither blockade of hGPV by LUM/B F(ab)₂ nor rhGPV (290 nM) affect thrombin time. (a, c, d, e) Values are displayed as mean ± SD. (d) n = 4 donors, 3 independent experiments, two-tailed unpaired t-test with Welch's correction. (e) n = 3 donors, one-way ANOVA. (f, g) Recalcified whole blood was incubated *in vitro* with 10 µg/ml anti-hGPV antibody LUM3 prior to perfusion over collagen/TF spots. Quantification time to fibrin formation (f) and fibrin surface coverage (g) during blood flow of LUM3-treated (n = 8 donors) and control samples (n = 10 donors). (f) n = 6 donors Values are depicted as mean ± SEM (g). SAC: Surface area coverage. Ctrl: Human donor.

Extended Data Table 1 | Analysis of platelet count, size, and surface expression of glycoproteins in *Gp5^{dThr}* mice

	WT	<i>Gp5^{dThr}</i>	P-value	Sig.
Count	85.8 ± 25.0	102.8 ± 20.4	0.2460	n.s.
MPV	5.4 ± 0.2	5.5 ± 0.2	0.4678	n.s.
WBC [10/ μ l]	76.7 ± 21.6	76.0 ± 15.2	0.95355473	n.s.
RBC [1E4/ μ l]	89.0 ± 25	93.2 ± 3.1	0.70015665	n.s.
HGB [g/dl]	1.4 ± 0.3	1.5 ± 0.1	0.43026063	n.s.
HCT [%]	4.8 ± 1.3	5.1 ± 0.2	0.52205469	n.s.
GPIb [MFI]	341.3 ± 20.3	354.3 ± 5.3	0.29312226	n.s.
GPV [MFI]	318.5 ± 11.9	289 ± 32.6	0.1203	n.s.
GPIX [MFI]	308.75 ± 8.66	317.75 ± 4.79	0.13244492	n.s.
GPVI [MFI]	33.25 ± 0.96	34 ± 1.41	0.41799623	n.s.
$\alpha_{IIb}\beta_3$ [MFI]	338.75 ± 27.68	353 ± 14.53	0.4216117	n.s.
β_3 [MFI]	157.8 ± 43.6	153.2 ± 5.7	0.8260	n.s.
α_5 [MFI]	18 ± 0.01	18 ± 0.032	1	n.s.
α_2 [MFI]	38.75 ± 0.957	39.25 ± 3.59	0.80343776	n.s.
CD9 [MFI]	669.75 ± 45.15	746 ± 2.83	0.04258772	*
CLEC-2 [MFI]	90.75 ± 6.24	82.5 ± 15.26	0.37396966	n.s.
CD84 [MFI]	25 ± 1.63	25.5 ± 0.58	0.59667799	n.s.

Mean platelet count and size were determined using a Sysmex cell counter. Surface expression of platelet glycoproteins was determined by flow cytometry. Diluted whole blood was stained with FITC-labelled antibodies at saturating amounts for 15 min at RT. Platelets were analysed immediately on a FACSCalibur. Results are expressed as mean fluorescence intensity (MFI) ± SD. n=4-6, two-tailed unpaired t-test with Welch's correction, *p<0.05.

Reporting Summary

Nature Portfolio wishes to improve the reproducibility of the work that we publish. This form provides structure for consistency and transparency in reporting. For further information on Nature Portfolio policies, see our [Editorial Policies](#) and the [Editorial Policy Checklist](#).

Statistics

For all statistical analyses, confirm that the following items are present in the figure legend, table legend, main text, or Methods section.

n/a Confirmed

- The exact sample size (n) for each experimental group/condition, given as a discrete number and unit of measurement
- A statement on whether measurements were taken from distinct samples or whether the same sample was measured repeatedly
- The statistical test(s) used AND whether they are one- or two-sided
Only common tests should be described solely by name; describe more complex techniques in the Methods section.
- A description of all covariates tested
- A description of any assumptions or corrections, such as tests of normality and adjustment for multiple comparisons
- A full description of the statistical parameters including central tendency (e.g. means) or other basic estimates (e.g. regression coefficient) AND variation (e.g. standard deviation) or associated estimates of uncertainty (e.g. confidence intervals)
- For null hypothesis testing, the test statistic (e.g. F , t , r) with confidence intervals, effect sizes, degrees of freedom and P value noted
Give P values as exact values whenever suitable.
- For Bayesian analysis, information on the choice of priors and Markov chain Monte Carlo settings
- For hierarchical and complex designs, identification of the appropriate level for tests and full reporting of outcomes
- Estimates of effect sizes (e.g. Cohen's d , Pearson's r), indicating how they were calculated

Our web collection on [statistics for biologists](#) contains articles on many of the points above.

Software and code

Policy information about [availability of computer code](#)

Data collection

Data were collected in Microsoft Excel (Microsoft Office 365 for Enterprise).

Flow cytometry

Platelets were analyzed using BD FACSCalibur and the CellQuestPro (v6.0) software.

Intravital imaging

Immunofluorescent images from live mice were acquired on a Zeiss Axiovert 200 using the Metamorph software (version 6.2r6).

Imaging of histological sections

Images of Carstairs stained sections were acquired on a Leica DMI400B using the Leica Application Suite (LAS) software (version 2.6.0.R1).

Imaging of thrombus and fibrin formation under flow

Fluorescent images during thrombus and fibrin formation were acquired on a Leica DMI6000 B using Leica Application Suite (LAS) X software (version 1.9.013747) equipped with a DFC 360FX camera.

Airyscan Zeiss imaging

Immunofluorescent images were acquired on a Zeiss LSM 980 Airyscan microscope using Zeiss ZEN software (version 3.2) in superresolution mode with the smart setup.

Data analysis

Flow cytometry

Data were analyzed using FlowJo (v10.7 and v10.8.1). A gating strategy is provided in the supplementary information.

Thrombin generation

Data was analyzed using Thrombinoscope™ software, version 5.0.0.742

Intravital imaging, Imaging of histological sections

Images were visualized, and analyzed using Fiji (Ref. 62; v2.1.0/1.53t).

Imaging of thrombus and fibrin formation under flow

Fluorescent images were processed on a Leica Thunder Imager DMI8 using the Leica Application Suite (LAS) X software (version 3.7) with the background subtraction method ICC (Instant Computational Clearing). The exported images were analysed for surface area coverage of fibrin formation with self-written Python scripts (Ref. 61). Python scripts are available at: <https://github.com/HeinzeLab/GPV-flowchamber>. Surface area coverage of fluorescent Z-GGR-AMC images (resembling activity of thrombin) was analysed with Fiji (Ref. 62; v2.1.0/1.53t).

Z-stacks of fixed thrombi and static fibrin polymerization samples were acquired at a SP8 confocal microscope (Leica SP8 inverted microscope, using Hyvolution mode, 63x, z-step: 0.1 µm. Images were deconvolved using Huygens Professional Software (v 21.04). The deconvolved data set was exported as Imaris file format and visualised with Fiji (Ref. 62; v2.1.0/1.53t).

Airyscan Zeiss imaging

Immunofluorescent images deconvolved on the fly using Zeiss ZEN software (version 3.2). Representative micrographs were analyzed using Fiji (Ref 62; v2.1.0/1.53t). Scripts are available at: <https://github.com/HeinzeLab/GPV-flowchamber>.

Analysis of LSFM brain images

Images were converted to the Imaris file format (Imaris 9.9, Bitplane, Oxford) for further processing, segmentation and analysis of vessel diameter.

Western Blot analysis

Western Blots were acquired at an Amersham Image 680 (GE Healthcare). Densitometry analysis was performed on tiff-images using the gel analyzer tool in Fiji (Ref. 62; v2.1.0/1.53t).

Statistical analyses

No statistical methods were used to predetermine sample size. Data were collected in Microsoft Excel and statistical analysis was performed using GraphPad Prism software version 7.03 and 7.05 (GraphPad Software).

For manuscripts utilizing custom algorithms or software that are central to the research but not yet described in published literature, software must be made available to editors and reviewers. We strongly encourage code deposition in a community repository (e.g. GitHub). See the Nature Portfolio [guidelines for submitting code & software](#) for further information.

Data

Policy information about [availability of data](#)

All manuscripts must include a [data availability statement](#). This statement should provide the following information, where applicable:

- Accession codes, unique identifiers, or web links for publicly available datasets
- A description of any restrictions on data availability
- For clinical datasets or third party data, please ensure that the statement adheres to our [policy](#)

Numerical Draw data are available in the main source data file corresponding to each figure text or the supplementary material information.

Human research participants

Policy information about [studies involving human research participants and Sex and Gender in Research](#).

Reporting on sex and gender

Sex was no criteria in study design, however, (based on self-reporting) both male and female healthy volunteers were included and no differences between sexes were noted in our assays.

Population characteristics

Healthy human volunteers (age range 18-65 years) were recruited with the following exclusion criteria:

- infection at time of blood taking
- any known pre-existing illness
- anti-platelet or anti-coagulant treatment during the last 14 days before blood taking

Ethnicity was not specifically taken into account, however, based on the recruiting environment (German University) ethnicity was predominantly White-European and the median age was 32 years.

Recruitment

The test persons were recruited via notices on notice boards of the University of Würzburg and University Hospital Würzburg as well as via notices in social media networks, which resulted in a potential bias towards "younger" adults and predominantly White-European ethnicity. However, as only treated samples were compared to vehicle samples (always from the same donor) this is unlikely to impact the effects of sGPV or anti-GPV on thrombus formation in our in vitro assays. The research protocol was approved by the Institutional Review Board and the need for individual informed consent was waived. No financial compensation was offered to participants.

Ethics oversight

The study complies with the Declaration of Helsinki and was approved by Institutional Review Boards (IRB, Ethikkommission) of University of Würzburg as stated in the methods section.

Note that full information on the approval of the study protocol must also be provided in the manuscript.

Field-specific reporting

Please select the one below that is the best fit for your research. If you are not sure, read the appropriate sections before making your selection.

Life sciences Behavioural & social sciences Ecological, evolutionary & environmental sciences

For a reference copy of the document with all sections, see [nature.com/documents/nr-reporting-summary-flat.pdf](https://www.nature.com/documents/nr-reporting-summary-flat.pdf)

Life sciences study design

All studies must disclose on these points even when the disclosure is negative.

Sample size	No statistical methods were used to predetermine sample size. Pilot experiments and previously published results were used to estimate the sample size, such that appropriate statistical tests could yield significant results. Sample sizes for in vivo experiments comply with the 3Rs rule on reducing, replacing and refining the use of animals for scientific purposes. The sample size (n) for each experiment is provided in the figure legends. For in vitro experiments, at least n= 3 mice per group were included and all experiments were performed at least twice.
Data exclusions	No data were excluded.
Replication	All experiments presented were conducted with sufficient mouse numbers to ensure statistical significance could be reached. Biochemical or image based data were reproduced in multiple mice/protein batches. Results shown are representative of several independently performed experiments. All attempts of replicating data were successful. Experiments were replicated at least once to ensure validity.
Randomization	All studies were performed with randomization when possible. For the treatment groups, mice were randomized cage-wise and experiments were performed in a blinded manner during experiments and outcome assessment. The distribution of the mice into different groups was randomized using research randomizer (randomizer.org). Randomization does not apply to experiments using human blood where the blood sample was divided into an untreated and treated sample after blood taking.
Blinding	All experiments were performed and analyzed in a blinded manner, e.g. by using code labeling for mice, sections or flow chambers.

Reporting for specific materials, systems and methods

We require information from authors about some types of materials, experimental systems and methods used in many studies. Here, indicate whether each material, system or method listed is relevant to your study. If you are not sure if a list item applies to your research, read the appropriate section before selecting a response.

Materials & experimental systems

n/a	Involved in the study
<input type="checkbox"/>	<input checked="" type="checkbox"/> Antibodies
<input type="checkbox"/>	<input checked="" type="checkbox"/> Eukaryotic cell lines
<input checked="" type="checkbox"/>	<input type="checkbox"/> Palaeontology and archaeology
<input type="checkbox"/>	<input checked="" type="checkbox"/> Animals and other organisms
<input checked="" type="checkbox"/>	<input type="checkbox"/> Clinical data
<input checked="" type="checkbox"/>	<input type="checkbox"/> Dual use research of concern

Methods

n/a	Involved in the study
<input checked="" type="checkbox"/>	<input type="checkbox"/> ChIP-seq
<input type="checkbox"/>	<input checked="" type="checkbox"/> Flow cytometry
<input checked="" type="checkbox"/>	<input type="checkbox"/> MRI-based neuroimaging

Antibodies

Antibodies used

Commercial antibodies:

PAC1-FITC: BD Biosciences, Cat. #340507, 15 µg/ml, 15 µl per test
anti-CD62P-APC: BD Biosciences, Cat. #550888, Lot: 0016310, 5 µl per test
control rat IgG: Sigma, Cat. #I4131, in vivo: 100 µg, in vitro: 10 µg/ml
anti-mGPV: R&D, Cat. #AF6990, dilution: 1:500
anti-hGPV: Santa Cruz, Cat. #sc271662, dilution: 1:200
platelet-depletion antibody: Emfret analytics, Cat. #R300, 0.14-0.18 µg/g body weight
Streptavidin: Thermo Scientific, Cat. #43-4301, in-house conjugated to HRP, dilution: 1:10000
anti-GAPDH: Sigma, Cat. #G9545, dilution: 1:3000
anti-mCD31: BioLegend, Cat. #102402, clone: 390, in-house conjugated to AF647, 0.4 µg/g body weight

antibody provided by W. Ruf:
anti-fibrin antibody: clone 59D8, conjugated to AF488, 1 µg/ml

in-house generated, purified and if indicated labelled mAbs
 all listed in-house generated antibodies/hybridomas were from Institute for Experimental Biomedicine, Würzburg, Prof. Nieswandt:
 anti-mouse P-selectin FITC, clone: WUG1.9, saturating amounts were used for flow cytometry, Ref. Schulte et al., Blood 2003, doi:10.1182/blood-2002-10-3242
 anti-mouse/human GPVI: clone JAQ1, saturating amounts were used for flow cytometry, in vivo: 100 µg, Ref. Nieswandt et al., J Exp Med 2001, doi:10.1084/jem.193.4.459
 anti-mouse GPIIb/IIIa-PE: clone JON/A, saturating amounts were used for flow cytometry, Ref. Bergmeier et al., Cytometry 2002, doi:10.1002/cyto.10114
 anti-mouse GPIX: clone p0p6, Ref. Stegner et al., Nat commun 2017, doi:10.1038/s41467-017-00201-7
 anti-mouse GPIX-FITC: saturating amounts were used for flow cytometry
 anti-mouse GPIX-A488:in vivo labelling: 1 µg/mouse
 anti-mouse GPIX-A405/A647: in vitro thrombus formation: 1 µg/ml
 anti-mouse GPV: clone DOM/B, in vivo: 100 µg, in vitro: 10 µg/ml, Ref. this study
 anti-mouse GPV DOM/B HRP: 1:1000
 anti-mouse GPV: clone DOM/C, in vivo: 100 µg, in vitro: 10 µg/ml, Ref. this study
 anti-mouse GPV: clone DOM3, in vivo: 100 µg, in vitro: 10 µg/ml, Ref. Nieswandt et al., Blood 2000, 96, 2520-2527
 anti-human GPV: clone LUM/B, in vivo: 100 µg, in vitro: 10 µg/ml, Ref. this study
 anti-human GPV: clone LUM1, 10 µg/ml, Ref. this study
 anti-human GPV : clone LUM2, 10 µg/ml, Ref. this study
 anti-human GPV: clone LUM3, 10 µg/ml, Ref. this study
 anti-human GPV: clone LUM4, 10 µg/ml, Ref. this study
 anti-human GPV: clone LUM5, 10 µg/ml, Ref. this study
 anti-mouse α2 integrin: clone LEN/B, 10 µg/ml, Ref. Shida et al., Blood 2014, doi:10.1182/blood-2013-09-521484
 anti-mouse GPIIbα: clone p0p/B, 10 µg/ml, Ref. Massberg et al., J Exp Med 2003, 197, 41-49
 anti-mouse GPIIbα-FITC: clone p0p4, saturating amounts were used for flow cytometry, Ref. Bergmeier et al., Blood 2000, 95, 886-893
 anti-mouse/human GPIIbβ: clone p0p1, Ref. Nieswandt et al., Blood 2000, 94, 684-693
 anti-mouse GPIIb/IIIa: clone JON1, saturating amounts were used for flow cytometry, Ref. Nieswandt et al., Blood 2000, 96, 2520-2527
 anti-mouse GPIIIa: clone EDL1, saturating amounts were used for flow cytometry, Ref. Nieswandt et al., Blood 2000, 96, 2520-2527
 anti-mouse Integrin α2: clone LEN1, saturating amounts were used for flow cytometry, Ref. Nieswandt et al., J Biol Chem 2000
 anti-mouse Integrin α5: clone BAR1, saturating amounts were used for flow cytometry, Ref. Grüner et al., Blood 2003
 anti-mouse CD9: clone ULF1, saturating amounts were used for flow cytometry, Ref. Nieswandt et al., EMBO 2001
 anti-mouse CD84: clone JER-1, saturating amounts were used for flow cytometry, Ref. Hofmann et al., J Thromb Haemost 2012
 anti-mouse CD105: clone MJ7/18, 0.14-0.18 µg/g body weight, Ref. Zehentmeier et al., Eur J Immunol 2014, commercially available at ThermoScientific Fisher, #14-1051-82

Validation

Validation of commercial antibodies was done on a regular quality control of each lot by the manufacturer. The anti-CD31 antibody was quality control tested by immunofluorescent staining with flow cytometry analysis. BDBiosciences further tests each lot of antibody to an internally established "gold standard" to maintain lot-to-lot consistency. They conduct wide-scale stability studies to guarantee an accurate shelf-life for their products.
 We tested new lots of commercial or in-house generated antibodies against a "gold standard" reference lot and tested against respective isotype controls. New antibodies for which no reference lot was available were validated in comparison to isotype controls and - where possible - with the help of samples from respective knockout animals.
 Additionally, our laboratory has utilized this panel of antibodies for intravital microscopy (Stegner et al. Nat Cardiovasc Res 2022) and flow cytometry antibodies in recent publications (Brown et al., Blood Advances 2022).

Eukaryotic cell lines

Policy information about [cell lines and Sex and Gender in Research](#)

Cell line source(s)

Sf9 insect cell line (ThermoFisher Scientific, #11496015)

Authentication

Sf9 cells were verified by ThermoFisher Scientific and quality control tested:
 - each vial contains 1×10^7 viable cells/ml
 - cells are negative for mycoplasma contamination
 - cells are tested negative for contamination with bacteria, virus and yeast
 - determined by isoenzyme and karyotype analysis

Mycoplasma contamination

Cells are certified from the vendor to be negative for mycoplasma contamination

Commonly misidentified lines (See [ICLAC](#) register)

No commonly misidentified lines were used for this study.

Animals and other research organisms

Policy information about [studies involving animals; ARRIVE guidelines](#) recommended for reporting animal research, and [Sex and Gender in Research](#)

Laboratory animals

All animals/mouse lines are described in detail in the Method section. For all experiments, male and female mice aged 4-20 weeks were used. All mice were kept on a C57B6/J background.

Gp5^{-/-} mice were kindly provided by François Lanza (Inserm-Université de Strasbourg, Strasbourg, France) (Kahn, M. L. et al., *Blood* 94, 4112-4121 (1999))
 Itga2^{-/-} mice were kindly provided by Beate Eckes (Department of Dermatology, University of Cologne, Cologne, Germany) (Holtkotter, O. et al. *J. Biol. Chem.* 277, 10789-10794, doi:10.1074/jbc.M112307200 (2002))
 Gp5dThr mice were generated (first description this study, Extended Data Fig. 01), intercrossed with Flip-positive mice to delete the Neo-cassette and backcrossed to C57Bl/6J background.
 RhoAfl/fl mice were kindly provided by Cord Brakebusch (University of Copenhagen, Copenhagen, Denmark) (Jackson, B. et al. *Mol. Biol. Cell* 22, 593-605, doi:10.1091/mbc.E09-10-0859 (2011)). To generate MK-/platelet-specific knockout mice, the floxed mice were intercrossed with mice carrying the Cre recombinase under control of the Pf4 (platelet factor) promoter. Nbeal2^{-/-} mice were described previously (Deppermann, C. et al., *J. Clin. Invest.* 123, 3331-3342, doi:10.1172/JCI69210 (2013)).

Wistar rats: strain: RjHan:WI, females, starting at 6 weeks of age, from Javier or Charles River
 Where appropriate, age- and sex-matched mice were used for experiments.

Wild animals

This study did not involve wild animals.

Reporting on sex

Female and male mice were used for experiments: where possible, a comparable percentage of female:male mice was used within one experiment for different (treatment/genotype) groups. No sex-based differences were observed during the study. For tMCAO experiments, only male mice were used to exclude different oestrogen levels as a confound.

Field-collected samples

This study did not involve samples collected from the field.

Ethics oversight

Animal studies and protocols were performed in accordance with German law and the governmental bodies and approved by the District of Lower Franconia as stated in the methods section. Animal experiments were performed in compliance with relevant ethical regulations and all efforts were made to avoid suffering of animals.

Note that full information on the approval of the study protocol must also be provided in the manuscript.

Flow Cytometry

Plots

Confirm that:

- The axis labels state the marker and fluorochrome used (e.g. CD4-FITC).
- The axis scales are clearly visible. Include numbers along axes only for bottom left plot of group (a 'group' is an analysis of identical markers).
- All plots are contour plots with outliers or pseudocolor plots.
- A numerical value for number of cells or percentage (with statistics) is provided.

Methodology

Sample preparation

Please see Method section for detailed information.
 Blood was drawn from the retro-orbital plexus in heparin and either directly diluted with PBS, stained with saturating amounts of the indicated antibodies (Glycoprotein expression) or blood/platelets were washed, stimulated with the indicated agonists and stained with saturating amounts of the indicated antibodies.

Instrument

Becton Dickinson FACSCalibur

Software

CellQuest Pro (v6.0) was used for data collection and FlowJo (v10.7, 10.8.1) for data analysis.

Cell population abundance

Cell population abundance: For in vitro experiments, population abundance of platelets was approx. 50%, for flow cytometry using whole blood, platelet population abundance was around 5% (lower for thrombocytopenic mice).

Gating strategy

Platelets were gated based on FSC/SSC characteristics. A gating strategy is provided in the Supplementary Information.

- Tick this box to confirm that a figure exemplifying the gating strategy is provided in the Supplementary Information.